JGR | Machine Learning and Computation

RESEARCH ARTICLE
10.1029/2025JH000584

Tropical Cyclone Surface Winds From Aircraft With a Neural Network

Alexander J. DesRosiers[1,2], Michael M. Bell[1], Jennifer C. DeHart[1], Jonathan L. Vigh[3], Christopher M. Rozoff[3], and Eric A. Hendricks[3]

[1]Department of Atmospheric Science, Colorado State University, Fort Collins, CO, USA, [2]Now at Cooperative Institute for Research in the Atmosphere, Colorado State University, Fort Collins, CO, USA, [3]U.S. National Science Foundation National Center for Atmospheric Research, Boulder, CO, USA

Key Points:

- Tropical cyclone (TC) surface wind reductions from aircraft observations vary with flight altitude, TC motion, and intensity
- A neural network (NN) trained with aircraft observations is used to improve the reduction of TC winds from flight level to the surface
- The NN can predict observed surface winds with greater accuracy and better structural asymmetry than the current operational procedure

Correspondence to:
A. J. DesRosiers,
adesros@rams.colostate.edu

Citation:
DesRosiers, A. J., Bell, M. M., DeHart, J. C., Vigh, J. L., Rozoff, C. M., & Hendricks, E. A. (2025). Tropical cyclone surface winds from aircraft with a neural network. *Journal of Geophysical Research: Machine Learning and Computation*, *2*, e2025JH000584. https://doi.org/10.1029/2025JH000584

Received 17 JAN 2025
Accepted 13 MAY 2025
Corrected 10 JUN 2025

This article was corrected on 10 JUN 2025. See the end of the full text for details.

Author Contributions:

Conceptualization: Alexander J. DesRosiers, Michael M. Bell
Data curation: Alexander J. DesRosiers, Jonathan L. Vigh
Formal analysis: Alexander J. DesRosiers
Funding acquisition: Michael M. Bell, Jonathan L. Vigh
Investigation: Alexander J. DesRosiers, Jennifer C. DeHart
Methodology: Alexander J. DesRosiers, Jennifer C. DeHart
Project administration: Michael M. Bell

Abstract Estimates of the surface wind field in a tropical cyclone (TC) are required in real time by operational forecast centers to warn the public about potential impacts to life and property. In-situ aircraft data must be adjusted from flight level to surface using wind reductions (WRs) since the aircraft cannot fly too low due to safety concerns. Current operational WRs do not capture all the variability in the TC surface wind field. In this study, an observational data set of Stepped Frequency Microwave Radiometer (SFMR) surface wind speeds that are collocated with flight-level predictors is used to analyze the variability of WRs with respect to aircraft altitude and TC storm motion and intensity. The Surface Winds from Aircraft with a Neural Network (SWANN) model is trained on the observations with a custom loss function that prioritizes accurate prediction of relatively rare high-wind observations and minimization of variance in the WRs. The model is capable of learning physical relationships that are consistent with theoretical understanding of the TC boundary layer. Radar-derived wind fields at flight level and independent dropwindsonde in-situ surface wind measurements are used to validate the SWANN model and show improvement over the current operational procedure. A test case shows that SWANN can produce a realistic asymmetric surface wind field from a radar-derived flight-level wind field which has a maximum wind speed similar to the operational intensity, suggesting promise for the method to lead to improved real-time TC intensity estimation and prediction in the future.

Plain Language Summary Extreme tropical cyclone (TC) winds can damage life and property. Aircraft provide useful data within TCs for forecasters to estimate the speed of damaging surface winds, but due to safety concerns much of the data comes from aircraft flight level several kilometers above the surface. Formulas for wind reductions (WRs) are used to reduce flight-level wind to its expected value at the surface. However, the actual WRs can vary with TC wind structure and storm motion, such that current operational WRs are not capable of accurately accounting for these complicating factors. In this study, these factors are analyzed and the results are used to train a neural network (NN) model with observational data to predict a surface wind field from aircraft observations and other TC information. The model is called Surface Winds from Aircraft with a Neural Network (SWANN), and it prioritizes accurate predictions of high-wind values given their importance to intensity estimation and damage potential. Validation of the model with data from past flights into TCs shows that SWANN improves on the current operational prediction formula. A test of a recent case shows SWANN is capable of producing accurate surface wind fields that can assist forecasters in real time.

1. Introduction

Operational forecasting centers such as the U.S. National Hurricane Center (NHC) are tasked with estimating and forecasting characteristics of the tropical cyclone (TC) surface wind field to warn the public on potential impacts and hazards. Accurate estimation of the maximum sustained, or 1-min average, wind speed of the TC at 10-m altitude in marine-exposure conditions (V_{max}) is important, yet it is almost never measured directly and instead must be estimated from remote sensing or proxy in-situ measurements above the surface. The most damaging winds are often located at the radius of maximum winds (RMW), typically located within the TC eyewall. In addition to the maximum wind, forecasters must estimate and forecast the radius of hurricane force winds (R64; 64 kt, where 1 kt $\sim$ 0.514 m s^{-1}), gale force winds (R50; 50 kt), and tropical storm force winds (R34; 34 kt) in quadrants to define the spatial distribution of the TC surface wind field (Sampson & Knaff, 2015). The intensity and wind radii are critically important for decision making by relevant partners and other users and therefore require as accurate an estimation as possible.

Software: Alexander J. DesRosiers, Michael M. Bell, Jennifer C. DeHart
Supervision: Michael M. Bell
Validation: Alexander J. DesRosiers
Visualization: Alexander J. DesRosiers, Jennifer C. DeHart, Christopher M. Rozoff, Eric A. Hendricks
Writing – original draft: Alexander J. DesRosiers
Writing – review & editing: Alexander J. DesRosiers, Michael M. Bell, Jennifer C. DeHart, Jonathan L. Vigh, Christopher M. Rozoff, Eric A. Hendricks

The TC surface wind maximum occurs within the turbulent planetary boundary layer (PBL) where reconnaissance aircraft cannot safely fly, which makes in-situ measurements of V_{max} difficult to obtain over the open ocean. In-situ wind observations are available at flight level along the flight track from U.S. Air Force Reserve Command (AFRC) C-130J Hercules and National Oceanic and Atmospheric Administration (NOAA) WP-3D (hereafter P-3) aircraft. Greater spatial coverage is possible when data from tail Doppler radars (TDRs) aboard the NOAA P-3 Hurricane Hunter aircraft are used for TDR-based 3-dimensional wind analyses in regions where scatterers are present (Lorsolo et al., 2013). TDR-based wind analyses cannot produce reliable winds near the surface due to partial filling of the radar beam by the surface and sea clutter at the lowest levels (DesRosiers & Bell, 2024). Estimates of surface wind can be obtained from aircraft observations by multiplying the flight-level wind by a wind reduction (WR) factor (e.g., Franklin et al. (2003); Powell et al. (2009)), which is the ratio of the surface wind speed to the flight-level wind speed. The focus of this study is to develop an improved formulation for WR using machine learning. Machine learning (ML) is gaining considerable traction for handling large data problems in atmospheric science (Boukabara et al., 2019). Recent success in accurately reconstructing the wind field structure of a TC using sparsely sampled data with a neural network (NN) demonstrates ML is a capable tool for this task (Eusbi et al., 2024).

Franklin et al. (2003) empirically derived WRs using wind profiles along the falling trajectories of Global Positioning System (GPS) dropwindsondes. Dropwindsondes can record wind measurements at frequencies of 2-Hz or 4-Hz, which may be representative of near-instantaneous higher gusts, so an average of the lowest 150 m of observed winds (WL150) is reduced to the surface using the profiles to obtain an estimate of the 1-min sustained wind. Advection of dropwindsondes as they fall from aircraft to the surface prevents their profiles from being truly vertical and makes the exact collocation of in-situ surface wind observations with flight-level wind observations impossible, so a statistical approach was used. The WRs calculated in Franklin et al. (2003) are valuable for operational V_{max} estimation at the NHC. However, these WRs were intended for locally determining V_{max} and significant radii from point measurements of wind, making them incapable of accounting for asymmetries in the full surface wind field of a TC.

A key mechanism that produces asymmetries in the surface wind field is variation in the frictional surface drag around the storm due to storm motion (Shapiro, 1983). TC-motion-induced asymmetries in the wind field result in asymmetric WRs around the TC with lesser reduction to the surface to the left of motion. This asymmetry in WRs was reasonably reproduced in a linear PBL model constructed by Kepert (2001) that produces an asymmetric jet due to strong inward advection of angular momentum and supergradient flow in the PBL. Nonlinear effects as well as vertical advection produce a stronger boundary layer jet and asymmetry that is more consistent with observed behavior (Kepert & Wang, 2001). The magnitude of storm motion and resulting surface drag asymmetries can move the surface RMW radially inward with increasing translation speed of a TC (Williams Jr, 2015). The outward slope of the TC eyewall is also important to inner-core WRs, as the maximum surface winds are almost always located radially inward of the flight-level RMW (Powell et al., 2009). Accurate prediction of WRs is a challenging, complex, and non-linear problem, which lends itself well to the strengths of ML over more traditional approaches.

Despite the challenges, operational estimation of the 2D surface wind field remains an important operational and research product. Most motion-induced asymmetry can be captured by first two azimuthal wavenumbers $0 + 1$ of the TC wind field (Uhlhorn et al., 2014), but additional asymmetries from internal dynamics and variations in surface characteristics can result in higher wavenumber structure. Knaff and Slocum (2024) designed an automated technique to reduce an observed flight-level wind field to the surface using an asymmetry-aware formulation of the Franklin et al. (2003) WRs employed operationally. Although this method is successful at producing bulk vortex surface wind field characteristics, its estimates of V_{max} are often too low, and its quality suffers when observational coverage is sparse. Kepert (2023) designed a parametric model capable of capturing impacts of increased surface roughness over land that increases frictional drag on the winds in the PBL. This method is an improvement in our understanding of frictional effects in the PBL, but is targeted for model assimilation into surge and wave models instead of operational intensity and wind radii estimation.

In this study, we utilize the Stepped Frequency Microwave Radiometer (SFMR), which is a nadir-looking airborne passive microwave radiometer that measures brightness temperatures (T_B) at six different C-band frequencies (Uhlhorn & Black, 2003; Uhlhorn et al., 2007). Although several other existing and emerging remote sensing technologies can be leveraged to estimate surface winds in TCs (Knaff et al., 2021), none match the sheer

quantity of surface wind estimates collocated with flight-level winds of the SFMR due to its use on the full fleet of AFRC C-130J and NOAA P-3 Hurricane Hunter aircraft over many years. Brightness temperatures recorded by the SFMR are sensitive to characteristics of the sea surface which changes in response to wind stress. The generation of sea foam and whitecaps from air mixing with ocean water at the surface (Holthuijsen et al., 2012) is the major contributor to variations in emissivity sensed by the SFMR, but other factors including sea surface temperature (SST) and column rain rate also influence the measurements. A geophysical model function (GMF), trained on dropwindsonde WL150 winds that incorporates SST and other additional information, relates rain rate and surface wind speed to emissivities. Surface wind speeds are retrieved via an inversion of the GMF forward model applied to the T_B sensed by the SFMR. SFMR surface wind estimates have uncertainties. Dropwindsondes drift downwind after deployment from the aircraft and measure a surface wind that is not collocated with the T_B footprint, in addition to other uncertainties in emission sources and instrument calibration.

The SFMR GMF has been improved through algorithm updates as well as characterization of its errors. Uncertainties in the partitioning of the measured emissivity in the retrieval algorithm can result in a high-wind-speed bias in heavy rainfall. Identification of these issues and reformulation of the GMF by Klotz and Uhlhorn (2014) greatly reduced this bias in the current retrieval algorithm. Sapp et al. (2019) investigated the current SFMR retrieval algorithm in use since 2016 and found several issues including a 10% low bias in predicted wind speeds below 45 m s^{-1} and low precision below 15 m s^{-1}. In this study, we use data from the latest version of the retrieval algorithm with the recognition that some uncertainty and potential low bias still remain.

In addition to retrieval uncertainty, sampling uncertainty is also an issue because the specific location where V_{max} occurs is rarely observed by the SFMR aboard aircraft, which cannot cover the entirety of a storm, resulting in a low bias of the peak observed wind. An observing system simulation experiment for the SFMR quantified the undersampling of V_{max} in modeled TCs by comparing the maximum winds recorded by the SFMR to the maximum winds of the modeled TC around the time of a simulated reconnaissance flight (Klotz & Nolan, 2019). The study found that in larger, weaker TCs of tropical storm intensity ($V_{max} < 65$ kt), the SFMR typically observed maximum winds less than V_{max} by 14% or more. As storms grow more organized and intense with compact inner cores, the underestimate is less pronounced with peak SFMR winds being lower than V_{max} in major hurricanes ($V_{max} \geq 96$ kt) by about 4% or less. In this study, we develop a NN that can be applied using Doppler-radar-derived winds at flight level, which helps to broaden the spatial coverage and reduce undersampling when TDR measurements are available.

Recent analysis has also discovered large random errors due to calibration errors across different SFMR instruments on TC reconnaissance aircraft (Chang & Jelenak, 2024). While these errors are very concerning for operational real-time use of individual SFMR units, we take advantage of the large database of past observations and NN techniques in order to reduce random error through averaging. We will demonstrate that our NN outperforms the current operational algorithm compared to independent dropwindsonde surface wind estimates despite all of the instrument, GMF, and sampling uncertainties from the SFMR.

This study provides a new ML algorithm that improves upon current operational WRs by better capturing the asymmetries and complexities of the flight-level and surface wind fields, which are critical to accurate surface wind reduction. The ML-model-derived surface wind fields produced by the method described herein can assist forecasters in real-time. Section 2 discusses the data and methods. In Section 3, the training data set is analyzed, different predictive NN methodologies are compared, and performance of the chosen NN model is evaluated. Discussion of the results and overall conclusions are given in Section 4.

2. Data and Methods

2.1. Aircraft Data

The Extended Flight Level Data set for Tropical Cyclones (FLIGHT+; Vigh et al., 2021) contains TC observations in a standardized format with flight-level and SFMR data collected during TC reconnaissance flights from 1997 through 2019 (version 1.3). Earth-relative and storm-relative winds are available at 1-s temporal resolution. The data are quality controlled and parsed into radial legs flown in toward or out from the TC center. The SFMR data in FLIGHT+ is reported as the wind speeds retrieved by the operational GMF at the time of a flight, so data collected prior to 2016 are omitted to ensure all surface wind data utilized in this study is retrieved from SFMR T_B using the most recent operational GMF (Klotz & Uhlhorn, 2014). SFMR data quality control during compilation

of the FLIGHT+ data set excludes observations collected when aircraft motion or shallow water conditions below the aircraft would impact the accuracy of the SFMR wind retrievals. The 1-s temporal frequency of the wind data results in a large spread of WRs due to gusty surface wind data within the PBL being more turbulent than the flight-level winds in the free troposphere (Zhang et al., 2011), among other factors. Extreme WR values may be due to observational errors and noise, and are not likely to be physically relevant to the relationships that a predictive methodology needs to learn to estimate surface winds. To remove extreme values, observations with WRs greater than 0.6 or less than 1.4 are removed from the data before any subsequent preprocessing steps. SFMR surface wind speeds greater than 90 m s^{-1} are also excluded due to being likely erroneous, given both the rarity of surface winds of this intensity and the limitations of the operational GMF at extreme winds (Klotz & Uhlhorn, 2014; Sapp et al., 2019).

The SFMR and flight-level wind data used in this study are then temporally smoothed to 10-s averages for all data points where the temporal window surrounding the observation reports values for at least 6 of the 10 s in the window. Some temporal autocorrelation is therefore present in this time series data, but accepted as a necessary shortcoming of the training data set to maintain a high volume of observations. To allow a ML method to predict winds in TCs across spectra of size and motion characteristics, observations are mapped to a normalized polar coordinate system on a flight-by-flight basis with coordinates of θ^* and r^*. The azimuthal θ^* direction is oriented by setting the TC motion direction to 0°. The TC motion direction is calculated using averages of the Cartesian zonal and meridional storm motion components, interpolated from wind centers, gathered during the time period spanning the initial time of the first radial leg to the final time of the last radial leg of a flight. Flights with storm motion magnitudes greater than 20 m s^{-1} are considered anomalous and excluded from the data set as outliers.

To obtain the normalized radius coordinate, r^*, the radial distance of an observation from the storm center is divided by the flight-level azimuthally averaged RMW calculated by averaging the radii with the maximum wind speed from each radial leg ($r^* = r/\overline{\mathrm{RMW}}$). RMW values greater than 100 km are typically indicative of weak storms with poorly defined wind field structure, so any flights with RMWs in excess of this value are not included. Data in the eye with r^* values less than 0.3 are excluded due to the presence of known erroneous SFMR estimates where the chaotic sea state and resulting white-cap coverage is not representative of the local wind stress (Uhlhorn & Black, 2003). An outer bound must be set to ensure the training data are likely to be within the TC environment. Given the need to forecast values for R34, the outer r^* bound is set to 5 which contains the majority (∼92%) of SFMR observations of 34 kt or greater. Weak winds where SFMR sensitivity to surface emission is poor (Sapp et al., 2019) must be limited, so SFMR surface wind values below 9 m s^{-1} are removed. This condition, paired with the lower data inclusion bound of 0.6 for observed WR, effectively excludes any data with flight-level wind speeds below 15 m s^{-1}.

The TC intensity itself contains useful information about the radial structure of the TC wind field, with sharper wind peaks and stronger gradients found near the flight-level RMW in more intense storms (Martinez et al., 2017). Historical TC intensity data are available at 6-hourly synoptic times in the HURDAT2 data set (Landsea & Franklin, 2013) for storms in the North Atlantic, eastern North Pacific, and central North Pacific basins, where TC reconnaissance is most common. During each flight in the data set, the TC intensity (reported in kt) for the closest previous synoptic time is assigned to all observations collected during the flight. By using the previous intensity estimate, this predictor provides valuable information which would be available in a real-time application of surface wind prediction. Typical operational TC reconnaissance flight levels are the 850 hPa pressure altitude (∼1,500 m) in storms of tropical storm strength or less ($V_{max} < 64$ kt) and the 700 hPa pressure altitude (∼3,000 m) in storms of hurricane strength or greater ($V_{max} \geq 64$ kt) (Knaff et al., 2021). Although not all reconnaissance flights take place at these operational levels, large departures from these pressure altitudes should be avoided in the training data. Observations with flight-level pressure values outside of a range from 600 to 900 hPa are therefore removed from the data set. The pressure-level filter removed all instances of storms below tropical storm intensity from the data set as weaker systems are often flown at lower levels. One other notable absence from the data set is Hurricane Dorian (2019) which would provide additional observations of extreme winds. Data from this storm was excluded due to evidence that the SFMR wind retrievals in this storm were problematic and inaccurate at high-wind values (Holbach, 2022).

After quality control, there are 808,215 samples available from model training and evaluation. When training ML models, it is important to set aside data to verify the model can generalize well and still achieve satisfactory performance scores on data not seen during training. To reduce spatial and temporal autocorrelation issues

10.1029/2025JH000584

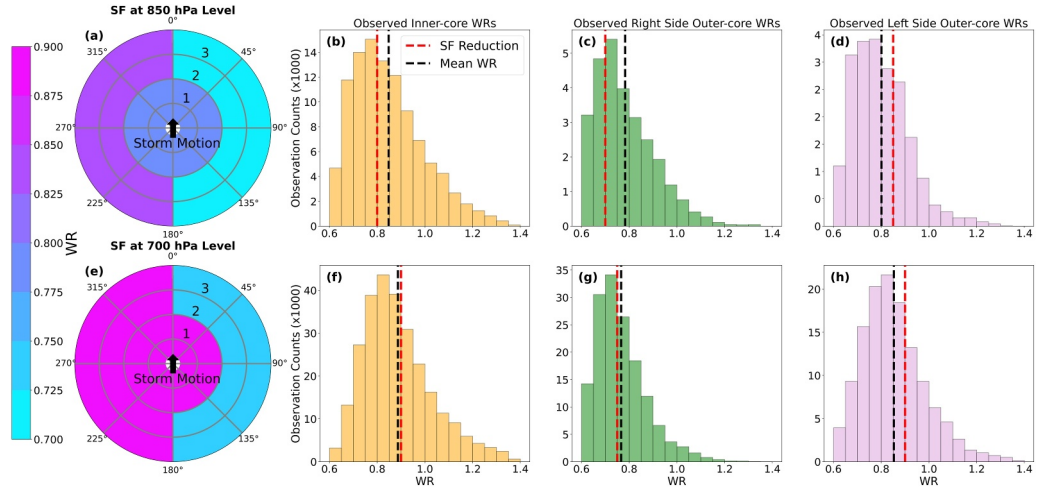

Figure 1. (a) Wind reductions ($\mathrm{WR} = \frac{\mathrm{SFMR\ Wind}}{\mathrm{Flight-level\ Wind}}$) recommended at the 850 hPa flight level by the Simplified Franklin (SF) wind reduction scheme. Histogram of all post-smoothing observed WR values in the data set with bin increments of 0.05 (b) within the TC inner core ($r^* < 2$) and (c) right side and (d) left side of the outer core ($2 \leq r^* \leq 5$) with the recommended SF WR (red dashed line) and mean WR of the distribution (black dashed line) shown in each. The same are provided for the 700 hPa level (e), (f), (g), and (h).

between the withheld sets and the training set, data from all flights into a single TC throughout its lifetime are kept together in whichever set they are assigned. The validation set (~8%) is composed of all observations collected in Hurricane Michael (2018), which was sampled by aircraft at a range of intensities from tropical storm to major hurricane (Beven et al., 2019). The testing set (~13%) consists of observations from Hurricane Matthew (2016), which was also sampled over a wide range of intensities (Stewart, 2017). The training set (~79%) is made up of the other 25 storms in the data set. Each of these data sets contains numerous observations of major hurricane force surface winds well in excess of 50 m s^{-1}.

2.2. The Simplified Franklin Wind Reduction Method

The WRs derived from dropwindsonde profiles by Franklin et al. (2003) are still used routinely in NHC operations and provide the benchmark for this study. Since their publication, NHC has introduced some modifications that allow forecasters to account, in a limited capacity, for motion-induced asymmetries. The operational method provides WRs which are differentiated by the inner core ($r^* < 2$) or outer core ($r^* \geq 2$), the presence of convection, left or right motion-relative location, and the pressure level of the observation. A Simplified Franklin (SF) wind reduction methodology is developed herein to resemble the current methodology at NHC and serve as a baseline of comparison for new methods evaluated in this study. Given the challenge of systematically determining the presence of convection, the SF method employed here always uses the WRs recommended for convection. We note that the operational WRs only deviate for non-convective areas in the outer vortex, so this approximation does not affect the inner core estimates. Although the SF method is a simplified version with respect to the convective assumption, it is also a broadening of the technique for use with a 2-D wind field versus point observations for which it was originally intended for.

The recommended SF WR for the 850 hPa (Figure 1a) and 700 hPa (Figure 1e) pressure levels are shown spatially in the normalized polar coordinate space. The spatial field is notably coarse with sharp changes at the radial and azimuthal boundaries between different WRs. These WRs are symmetric in the inner core, offering new methods an opportunity for improvement relative to SF by more accurately accounting for TC eyewall asymmetries. Figures 1b–1h shows histograms of observed WRs within the TC inner core and the left and right sides of the TC outer core observed within 25 hPa of each pressure level. The mean WR values (black dashed lines) of the distributions are relatively close to the SF values (red dashed lines), indicating the SF technique is generally consistent with the mean of SFMR-derived WRs; however, the histograms show considerable spread about the fixed WR values of the SF method and exhibit positive skewness, offering possibilities for improvement to capture this variability with an approach that employs ML.

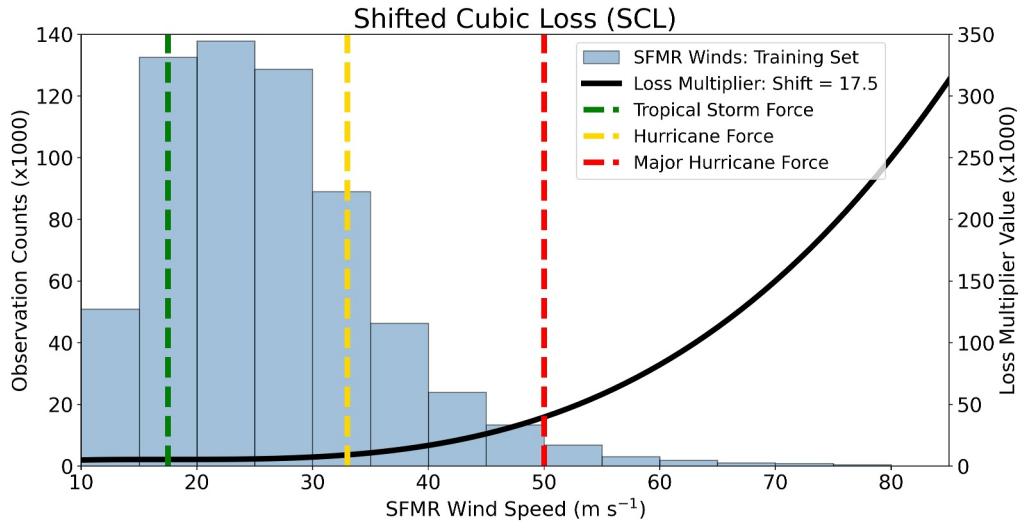

Figure 2. Histogram of observed SFMR wind speeds in the training set in 5 m s^{-1} increment bins. Multiplier values for traditional loss functions from shifted cubic loss (SCL; black line) in relation to the SFMR wind speed of an observation with tropical storm force (green dashed line; ∼17.5 m s^{-1}), hurricane force (yellow dashed line; ∼33 m s^{-1}), and major hurricane force (red dashed line; ∼50 m s^{-1}). The shift constant in the SCL function (Equation 1) is set to 17.5 m s^{-1}.

2.3. Machine Learning Architecture

An artificial neural network (NN) ML model (LeCun et al., 2015) is implemented using TensorFlow (Abadi et al., 2016) to capture complex relationships and predict surface winds from flight-level input features. The NN is a multi-layer perceptron that processes input features through successive hidden layers which connect to an output layer for the desired predictand, which can either be a WR or the surface wind itself. The NN consists of an input layer, which is the size of the given features, hidden layers which can vary in both number of layers and number of nodes per layer, and a single-node output layer. Unless otherwise noted, different techniques tested in this study use a NN architecture defined by two hidden layers with counts of 30 and 10 nodes respectively. The feed-forward network fully connects all nodes in the prior layer to the next layer moving information from the inputs, to the hidden layer(s), and finally the output. The nodes in each layer are assigned activation functions, which are applied to transform the incoming numerical information before passing it on to the next layer. Two safeguards are in place within the NN to prevent overfitting to the training data set, which can result in a model that does not generalize well to unseen data. A ridge regression (L2) coefficient is set in the hidden layers and the dropout technique is also applied to randomly drop nodes at a specified rate from the neural network during training (Srivastava et al., 2014). The L2 regularization penalizes large weights, reducing the influence of individual features, while dropout prevents the model from over-relying on specific nodes. Default hyperparameter choices for the tested methods are 50 epochs, batch size of 256, L2 regularization coefficient of 0.01, dropout rate of 0.2, rectified linear unit (ReLu) activation functions, and a conservative learning rate of 1×10^{-4}.

The loss function is important to how a NN learns and a common choice is minimizing the mean squared error (MSE) between the predicted and true values of the training set. In some cases, standard loss functions like MSE do not meet the needs of the problem and creation of a custom loss function is necessary to ensure the model learns appropriately (Ebert-Uphoff et al., 2021). One challenge presented by the current WR problem is the rarity of extreme-wind observations. Figure 2 shows a histogram of the SFMR surface wind speeds in the training data set, which is characterized by a higher concentration at wind speeds below 35 m s^{-1}. Early tests with a standard MSE loss function indicated that NNs significantly underestimated high-wind predictions due to this skewness (not shown). Since the determination of V_{max} in extreme TCs is an important aspect of our use case, a multiplier for the MSE was developed to increase the penalty for inaccurate predictions of high surface winds in the data set. The shifted cubic loss function (SCL) is defined as:

$$\text{Shifted Cubic Loss} = \text{MSE} \times \left((\text{SFMR} - \text{Shift})^3 + \text{Shift}^3\right) \quad (1)$$

Table 1
Neural Network Predictors

Predictor	Description
r*	RMW-normalized Radius of Observation
sin (θ*)	Sine of the Motion-relative Azimuth of Observation
cos (θ*)	Cosine of the Motion-relative Azimuth of Observation
V_{storm}	TC Translation Speed
V_{FL}	Observed Flight-level Wind Speed
H	Aircraft Altitude
V_{max}	TC Intensity at Prior Synoptic Time

where the shift value is subtracted from the SFMR 'truth' wind speed value in m s^{-1} and cubed. The cubed shift value is added to this quantity and the full value is multiplied by the MSE for each observation. The SFMR value makes the multiplier grow cubicly at high winds. The shift value, in this case set to the minimum tropical storm force wind value of 17.5 m s^{-1}, delays the cubic growth by shifting the inflection point between positive and negative decay away from zero and extends the relatively flat portion of the function through the commonly observed wind speed regime (Figure 2; black line). Adding the cubed shift value again in the multiplier shifts the inflection point upward and ensures the multiplier stays positive, even when SFMR values are less than the assigned shift value. The function essentially counters the rapid decrease of the number of observations at high winds with a rapid increase of loss penalty value in this region.

The NN is given a set of predictors, or features given in Table 1, with which to predict either the observed SFMR surface wind speed or WR. The location of the aircraft is provided in r* and θ* coordinates with both the sine and cosine of θ* given to prevent a jump discontinuity in predictions where θ* is equal to 0° at the normalized azimuth of storm motion. To capture the motion-induced asymmetry, the location information is necessary. The magnitude of the storm motion is also included which contributes to the magnitude of the motion-induced asymmetry (Kepert, 2001; Shapiro, 1983) and WRs (Powell et al., 2009). The flight-level wind and altitude of the aircraft are provided to inform the model of the value to be reduced and the height from which to reduce it. The intensity of the TC assessed at the prior synoptic time provides implicit information on the structure and symmetry of the TC wind field. All input features are standardized using their means and standard deviations in the training data set, which is required for satisfactory NN performance. The predictands, either SFMR wind speed or WR, are not standardized nor are they required to be.

2.4. Model Validation With Dropwindsondes

In this study, we validate with in-situ measurements from dropwindsondes that the model has never seen and are not collocated in space with any of the training data due to their drift from the flight track. The Tropical Cyclone Dropsonde Research and Operations Product Suite data set (TC-DROPS; version 1.2) contains a large collection of dropwindsonde profiles collected from 1996 to 2021 (Zawislak et al., 2018). A sustained surface wind is estimated from dropwindsonde descending profiles by reducing the WL150 mean wind to the surface consistent with the methodology described in Franklin et al. (2003). Surface wind observations derived from WL150 values calculated with TC-DROPS are also mapped to the normalized polar grid space using storm motion and RMW information from FLIGHT+.

To obtain the input flight-level wind, we use the Tropical Cyclone Radar Archive of Doppler Analysis with Re-centering (TC-RADAR; v3k) which is a historical data set of kinematic analyses produced via dual-Doppler wind synthesis of TCs observed with TDR between 1997 and 2022 (Fischer et al., 2022). Flight-level wind fields for storms of tropical storm strength (altitude = 1.5 km) and hurricane or greater strength (altitude = 3 km) are transformed to the normalized polar grid space for prediction of a surface wind field by the ML method. The wind fields are smoothed to WN 0 + 1, which was deemed adequate for capturing storm-scale wind asymmetries (Uhlhorn et al., 2014). The smoothing is carried out at each radius where 25% of the azimuths report wind data anywhere within the storm based on recommendations for allowable gap size, described by Lorsolo and Aksoy (2012). We note that this radar-derived wind represents a much coarser spatial and temporal footprint than the 10-s averaged in-situ wind used for training. Additionally, the dropwindsondes and TDR winds are not exactly collocated in time due to the temporal averaging of TDR winds over the course of the flight. While the wind features are being verified in the same storm-relative polar grid space, the presence of transient features in the real storm will necessarily introduce variability. Despite these discrepancies, the radar and dropwindsonde data sets allow for 1,151 points for an independent validation of the NN and comparison with the SF method used in operations.

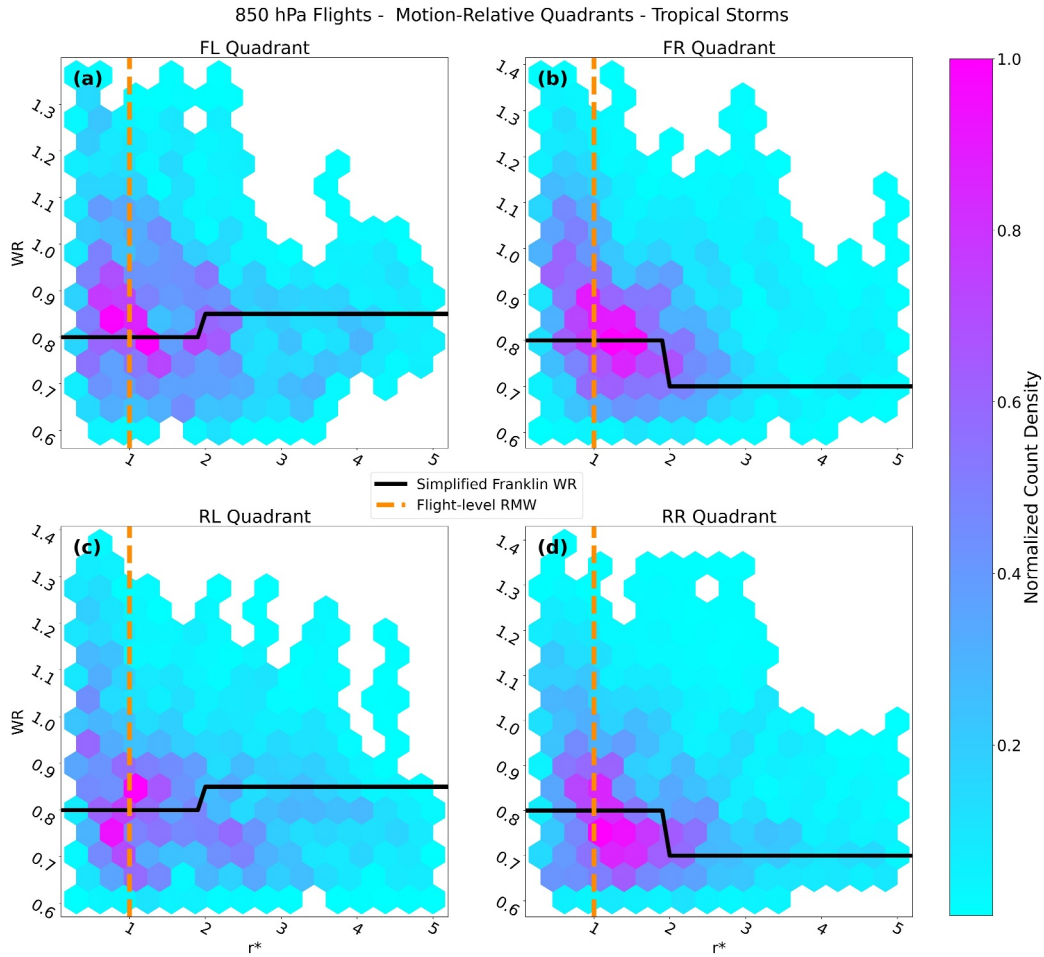

Figure 3. Hexbin plots with normalized density of observations in bins defined by coordinate pairs of wind reduction ($WR = \frac{SFMR\ Wind}{Flight-level\ Wind}$) and radial r* locations for flights in tropical storms ($V_{max} < 33$ m s^{-1}) at the 850 hPa pressure altitude. Observation densities are given in storm-motion-relative quadrants of front left (a; FL), front right (b; FR), rear left (c; RL), and rear right (d; RR). The recommended SF reduction (black line) and flight-level RMW (orange dashed line) are shown. An absence of hexbin tiles indicates no observations are present in that bin.

3. Results

3.1. Observed Wind Reduction Analysis

We first investigate the radial distribution of WRs in storm-motion-relative quadrants to help characterize the asymmetries the model is expected to learn from the observations and predict. The motion-relative quadrants are the front left (FL; $270° \leq \theta^* < 360°$), front right (FR; $0° \leq \theta^* < 90°$), rear right (RR; $90° \leq \theta^* < 180°$), and rear left (RL; $180° \leq \theta^* < 270°$). Hexbin plots are utilized to show the density of observations in the data set within bins defined by WR and r^* for each quadrant. The hexbins are made up of a 15 by 15 array of equally spaced bins in r^* values (0.3–5) and WR values (0.6–1.4) which makes for a total of 225 possible hex tiles in the plots. The density count in the analysis is normalized by the maximum value in each quadrant, which allows for a common color scale to better show the variance in each quadrant. The RMW (orange dashed lines) and WRs from the SF method (black lines) are overlaid to provide context of the TC structure and current operational methodology.

Figure 3 shows observations from flights into TCs of tropical storm intensity near the 850 hPa pressure altitude. The WRs near the RMW are concentrated around 0.8–0.9 in the front quadrants, with slightly lower WRs in the rear quadrants on average. There is also a weak left-to-right asymmetry, with slightly smaller WRs on the right side on average. There is a large amount of spread with values found anywhere in the allowed range of 0.6–1.4. Radially, the greatest density of observations is located within 2 r^*, likely due to the fact that the RMW is

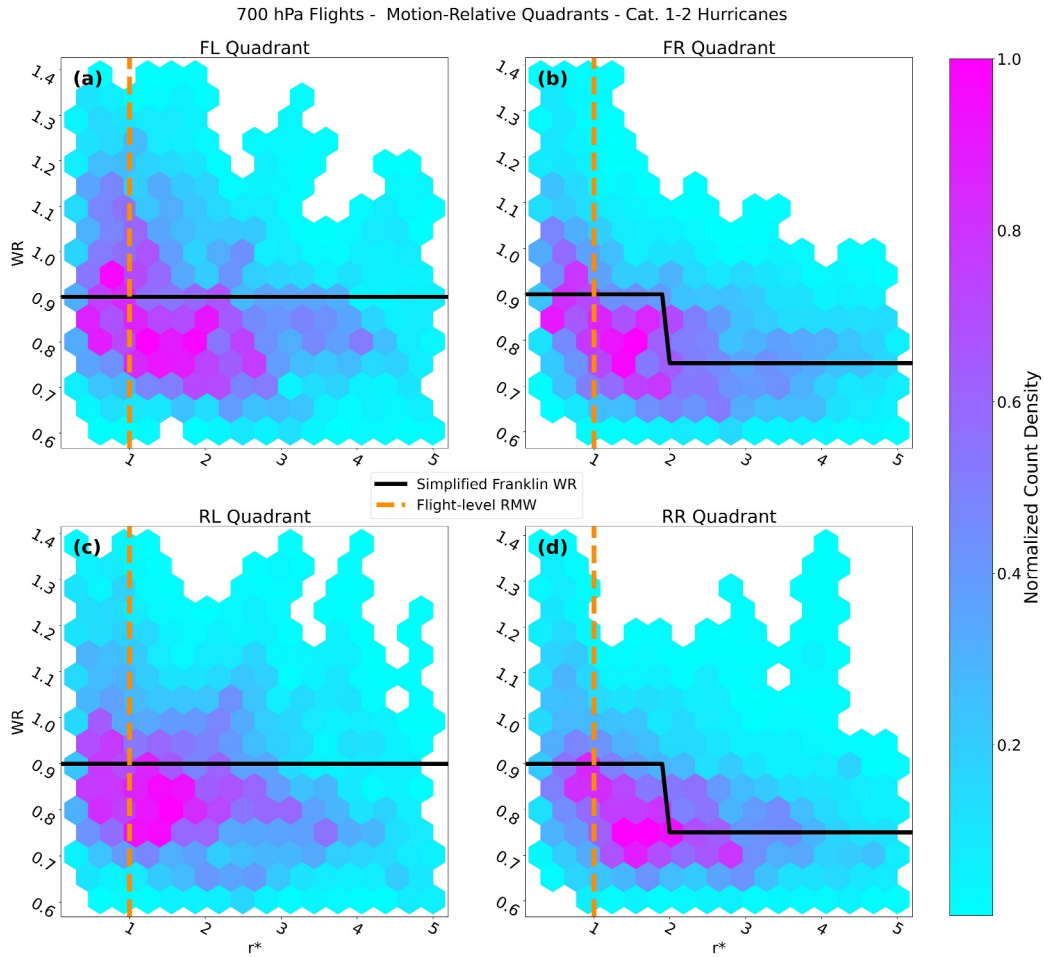

Figure 4. Same as Figure 3, but for 700 hPa pressure altitude flights into storms of Category 1–2 hurricane intensity (33 m s^{-1} ≤ V_{max} < 50 m s^{-1}).

typically larger in weaker storms (Fischer et al., 2022), making for a greater physical distance spanned per unit of r^*. The SF method line generally cuts through regions of high WR density, although the line is slightly higher than the maximum density in the RR quadrant. The decrease in SF WR on the right side at 2 r^* appears to be a reasonable match to the distribution. The left side increase in SF WR is more difficult to justify due to the large spread of possible values.

There is a more defined negative slope of WR with r^* near the RMW in Category 1 and 2 hurricanes observed by aircraft flying near the 700 hPa pressure altitude (Figure 4). The increasingly symmetric wind field in all four quadrants is consistent with behavior in observed TCs as they grow more intense (DesRosiers et al., 2022). The SF WR is generally near the upper end of the maximum density of observed values. The spread of WRs remains quite large in all quadrants, but is more concentrated near 0.8–0.9 than in the tropical storm cases.

In storms of major hurricane intensity observed by aircraft near the 700 hPa flight level (Figure 5), there is a well-defined negative slope of WR with r^* in the right quadrants and a flatter slope in the left quadrants. The bulk of RMW contraction typically takes place prior to TCs reaching major hurricane intensity (Stern et al., 2015), so the shrinking of physical space spanned by r^* coordinates between Figures 4 and 5 should be minimal. The greater normalized density in outer-core observations is likely due to outward expansion of the wind field. Similar to Category 1 and 2 storms, the greatest density of observed WRs is typically below the SF values throughout most of the storm. This stems from the original WRs in Franklin et al. (2003) being derived from averages, which are likely to be higher than the values found in the area of greatest density in a skewed distribution (Figure 1). We also emphasize that the basis of the SF method is intended for point reductions, and the observations are generally

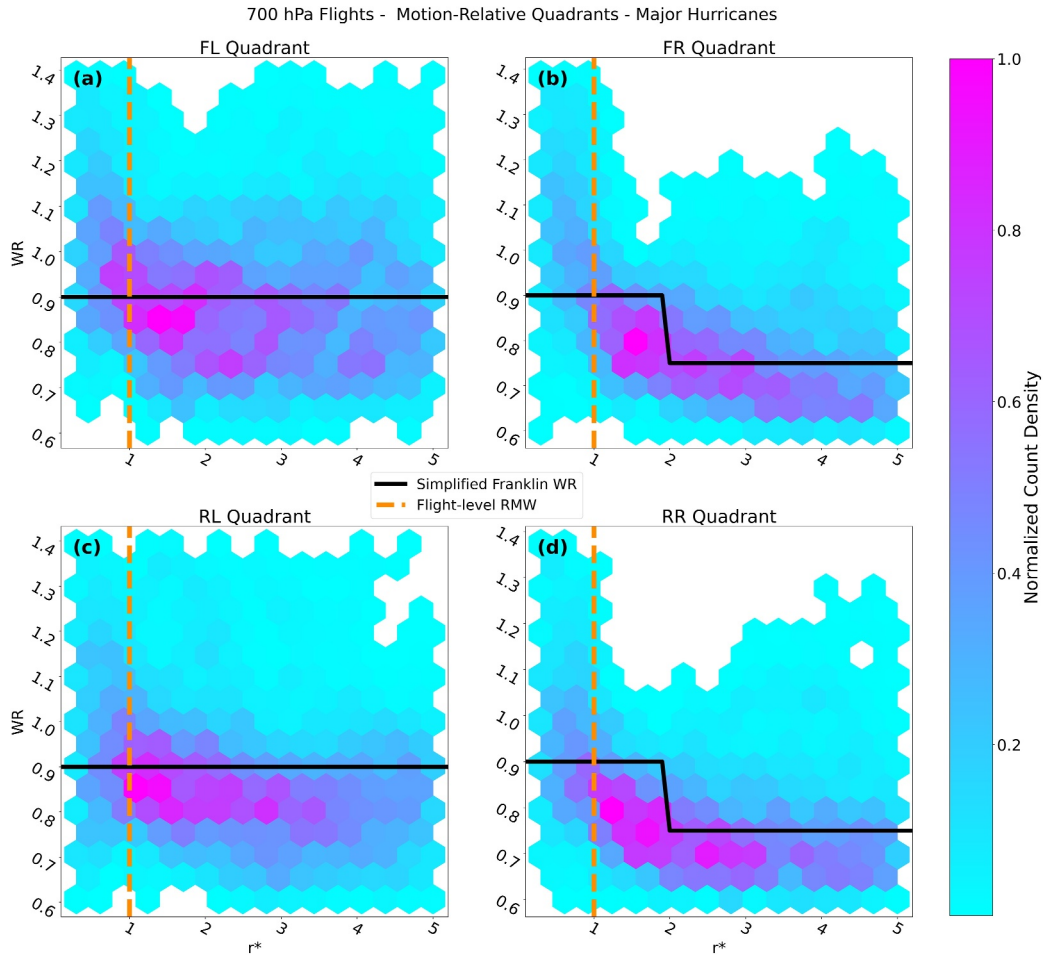

Figure 5. Same as Figure 3, but for 700 hPa pressure altitude flights into storms of major hurricane intensity ($V_{max} \geq 50$ m s^{-1}).

consistent with the SF values for the bulk of observations near the flight-level RMW. However, within the RMW, the SF recommendation is too low due to rising WRs likely caused by the outward slope of the TC eyewall with height (Hazelton & Hart, 2013). Due to this slope, the aircraft is likely to enter the eye and no longer observe strong winds at flight level while the SFMR continues to observe an ocean surface stressed by strong winds within the eyewall. This behavior is also noted in Powell et al. (2009), where the SFMR surface wind maximum was almost always located inward of the flight-level RMW. An increase in occurrence of higher WRs in the outer core may be related to the presence of cross swell in the far field of TCs which impacts the surface emissivity sensed by the SFMR (Holthuijsen et al., 2012).

The observed asymmetries in WRs suggests they are sensitive to both motion and the intensity of the system. An apparent increase in mean WR near and inward of the RMW should be accounted for with increasing WRs in this region to accurately place a surface wind maximum inward of the flight-level RMW. Overall, the variability of WRs in observed TCs derived from SFMR limits the applicability of fixed WRs such as those recommended by the SF method. This variability motivates the use of a more sophisticated method for wind reduction which can learn from and account for relationships present in the observations.

3.2. Neural Network Results

Several different combinations of loss functions and predictands were evaluated to identify the NN method best suited for wind reduction. The nomenclature for each NN version in this section is the loss function used in training followed by the predictand the model produces as its output. For example, a model referred to as MSE

Table 2
Key for the Neural Networks Nomenclature

Model name	Loss function	Predictand
MSE ERR	Mean Squared Error	Error (SFMR - SF Wind)
MSE WR	Mean Squared Error	Wind Reduction
MSE SFMR	Mean Squared Error	SFMR Surface Wind
SCL SFMR	Shifted Cubic Loss with MSE	SFMR Surface Wind
SCL WR	Shifted Cubic Loss with MSE	Wind Reduction

WR minimizes the mean squared error loss function in training and outputs a prediction for the WR to be used to relate the flight-level wind to the surface wind for the observation. In the case of a model prediction of WR, the NN is validating its prediction against the corresponding observed WR value. The different configurations use either a MSE loss or the SCL custom loss described in the methods section that increases the importance of accurate predictions in strong winds. The different possible predictands are the SFMR wind speed, the WR, and the residual error between an observed SFMR wind value and the predicted wind value from the SF method. A key for model nomenclature is given in Table 2. Note that for the error model, the predictand can be positive or negative. For the error NN (MSE ERR), the ReLu activation function, which limits output to positive values, is replaced by a hyperbolic tangent function, which allows the NN to produce negative output. The true error values in the data set are also scaled between −1 and 1 based on the minimum and maximum values found in the training set. The same scaler is applied to output from the NN to revert the unitless scaled errors back to values in m s^{-1}.

Performance of each method is evaluated with the testing set by comparing the true SFMR values to the SFMR wind speeds predicted by the NNs (Figure 6). For models predicting the WR, the predicted value is multiplied by the flight-level wind speed to obtain a predicted SFMR surface wind speed. Error predictions are added to the surface wind speed predicted by the SF method to obtain a predicted SFMR wind. Converting all predictions to a common target value allows for a more direct comparison of model accuracy. The MSE ERR, MSE WR, MSE SFMR, and SCL SFMR methods were all tested using the same NN settings and hyperparameters. The models generated by all methods, with the exception of MSE ERR, achieved both linear correlations, via r^2, and root mean squared error (RMSE) values that outperform the SF method (Figure 6). The MSE ERR method likely needs additional dedicated tuning effort due to its differences from the others, but this method was not pursued further in favor other techniques.

Among the top models, certain tradeoffs are apparent in their performance. The MSE SFMR method was consistently biased low in the rarely observed major hurricane force (SFMR wind ≥ 50 m s^{-1}) wind regime. The MSE WR method exhibited decreased low bias at high winds compared to MSE SFMR with similar performance metrics, but still struggled to predict high winds. The SCL SFMR model, which applies stronger weighting to

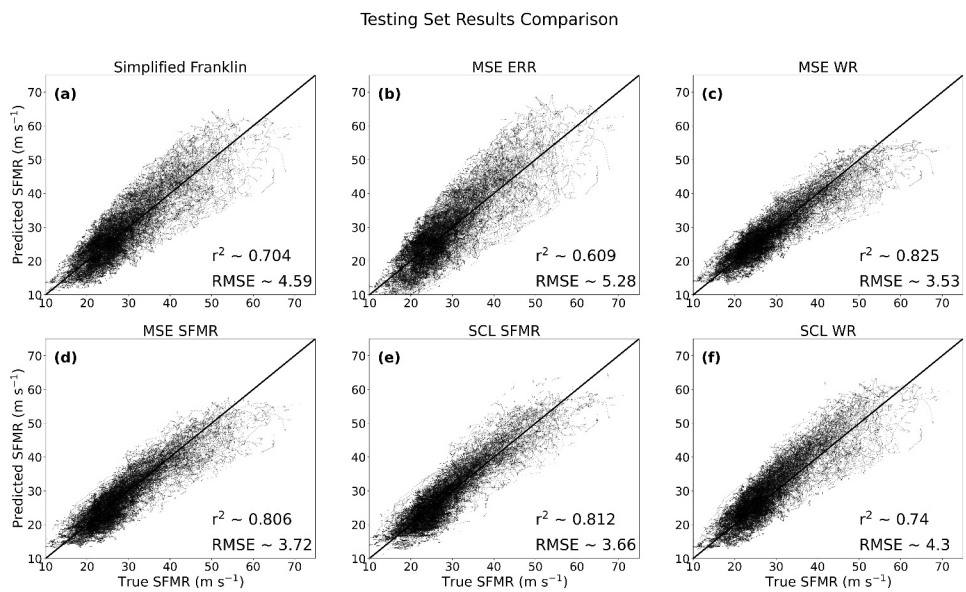

Figure 6. Predicted versus observed SFMR wind speeds with linear correlation (r^2) and root mean squared error (RMSE) values from the testing set given for the (a) SF, (b) MSE ERR, (c) MSE WR, (d) MSE SFMR, (e) SCL SFMR, and (f) SCL WR prediction techniques.

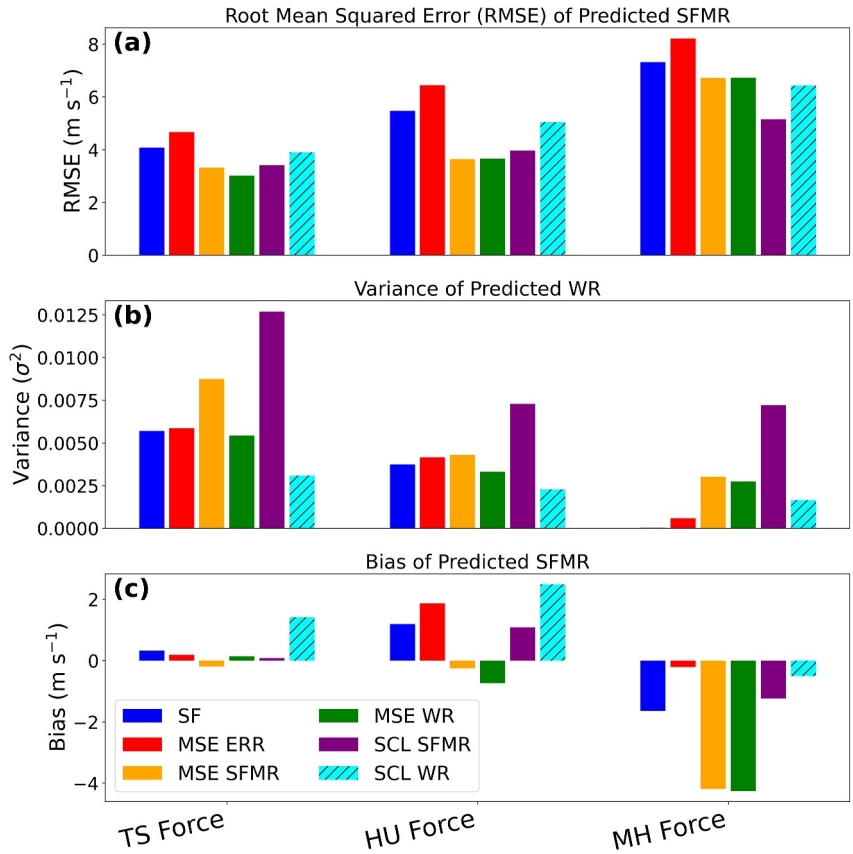

Figure 7. (a) Root mean squared error (RMSE) of predicted SFMR wind speeds versus observed, (b) variance (σ^2) of the predicted WRs, and (c) bias of predicted SFMR for each technique (legend) at SFMR wind speed forces of tropical storm (TS), Category 1–2 hurricane (HU), and major hurricane (MH) in the testing set.

high-wind observations in the loss function, is able to more accurately predict high SFMR surface winds, but in a manner which may be too constrained to noise in the SFMR.

Ideally, a WR model trained on observations should make skillful predictions of SFMR surface winds while also limiting the spatial variability in WR to produce a subjectively smooth analysis field. A model that has too much spatial detail in WR would not be desired by forecasters as large variance is likely evidence of a model which recreates the noise and biases of SFMR observations and departs from boundary layer theory (Kepert, 2001). At major hurricane force, the SCL SFMR model exhibits the lowest RMSE which demonstrates the effect of weighting the loss function by high SFMR values, and the other models are comparable in RMSE. However, when the spatial variance is maximized in all wind speed bins by the SCL SFMR model, which indicates the model may be learning too much noise from the SFMR instrument (Figure 7b). Conversely, the MSE WR model exhibits the best performance with respect to variance across all bins among the three. However, that model's underprediction of high winds is problematic.

To select the optimal model, we would like to balance all three constraints of a low RMSE, low variance, and accurate V_{max} in strong TCs. The SCL WR method meets this goal most effectively, and outputs a predicted WR, but is trained using SCL custom loss. The SCL formulation (Equation 1) for this model solves for MSE with true versus predicted WR values and multiplies the error by SCL which is still scaled by the SFMR value. The success of this NN training method prompted a more committed tuning effort to maximize performance. Hyperparameter tuning was performed with the KerasTuner package in Python (O'Malley et al., 2019). The number of hidden layers, number of nodes in each hidden layer, ridge regression coefficient, learning rate, and dropout rate were all allowed to vary, creating a multidimensional search space of the changing hyperparameter settings. KerasTuner returned an optimal model configuration with one hidden layer containing 20 nodes, a learning rate of $\sim 5.1 \times 10^{-5}$, a ridge regression coefficient of 0.2, and a large dropout rate of 0.4. The model was

allowed to run for 500 epochs with the small learning rate. Training was deemed complete by epoch 94 via an early stopping condition which monitors when the loss value in the validation set calculated after each epoch begins to consistently increase. The tuned SCL WR model has lesser accuracy scored by the RMSE of SFMR winds than the three most competitive models of the five originally tested (Figure 7a), but its variance in predicted WR is lower and decreases at higher wind speeds (Figure 7b). Furthermore, the model has a minimal low bias in major hurricane force winds (Figure 7c).

The performance metrics of the SCL WR model are slightly lower than those of the other methods with respect to its surface wind predictions in the testing set (Figure 6e). However, the SCL WR model successfully combats the low bias at high winds most models struggle with while maintaining considerable scatter about the 1-to-1 line at high winds where SFMR winds are uncertain. The trade-off with the skill at higher wind speeds is a ∼1–2 m s^{-1} high bias at lower wind speeds (Figure 7c). This high bias may be a necessary compromise in creating a model for surface wind reduction that can be helpful for real-time V_{max} estimation based on observations which may not contain V_{max}. The trade-off may be acceptable when considering the decrease in SFMR-based intensity underestimation with increasing storm intensity, characterized by Klotz and Nolan (2019), and the low bias in retrieved SFMR winds below 45 m s^{-1} (Sapp et al., 2019). We note that at all wind speeds the SCL WR model is more accurate than the operational SF method.

To better visually compare the model performance, Hurricane Zeta (2020) was selected from the TC-RADAR data set. Reconnaissance aircraft sampled Zeta with TDR at Category 1 intensity with a surface V_{max} of 80 kt (Blake et al., 2021), which is approximately 41 m s^{-1}. The flight-level RMW determined via the TDR data is 44 km and the forward motion is ∼7.5 m s^{-1} at 344° with respect to 0° set as north. The surface wind fields produced for the Hurricane Zeta case by the most competitive methods are shown in Figure 8. The SF method produces the strongest estimate of V_{max}, which is within 2 m s^{-1} of the intensity assessed by the NHC, but the wind maximum is located directly below the maximum at flight level which is unlikely due to the slope of the eyewall with height. The fixed nature of the SF method also maintains the asymmetry of the flight-level wind to the surface in the inner core while producing discontinuous transitions at the outer-core boundaries. The MSE WR and SCL SFMR methods show more symmetric surface wind fields with maxima located inward of the flight-level RMW. Despite the improved representation of general expected characteristics of the surface wind field, the maxima predicted by these two methods are much lower than that of the SF method. The V_{max} value of the SCL WR surface wind field is ∼3 m s^{-1} off from the operational estimate at this time, which has its own uncertainties. Although it is slightly weaker than the SF method maximum, the method captures the increased symmetry of the inner-core surface winds and inward displacement of the strongest winds from the flight-level RMW, which is believed to be a better representation of the TC structure. The Zeta case results also indicate the method fails to shift the surface wind maximum downwind of the flight-level wind maximum, a behavior expected in Kepert (2023). This failure may relate to sampling geometries. Azimuthal offsets may be too challenging to capture with vertically aligned training data.

Returning attention to the larger sample of cases, an additional evaluation is performed to compare the three most competitive NN models to the SF method in the ability to estimate the V_{max} operationally. For each merged case from the TC-RADAR data set, the flight-level wind field along with other necessary predictors is fed to each model to generate a surface wind field. The maximum value of that surface wind field is then compared to the NHC best track intensity at the time of analysis in TC-RADAR. The comparisons of predicted to actual intensity are shown for each method in Figure 9 where wind speed values are reported in knots in accordance with operational procedures. The MSE WR and SCL SFMR models consistently underpredict V_{max} with the greatest errors found in cases of major hurricane intensity. The SCL WR method decreases this bias with greater performance in stronger storms. Performance metrics, shown in each panel of Figure 9, are nearly identical for both the SF and SCL WR methods. The similarity in performance indicates the SCL WR method offers a more realistic representation of the surface wind field, as in the Zeta case (Figure 8), while giving comparable intensity estimation performance to the current operational procedure. Based on the above evaluation, we believe the SCL WR model is found to be the most suitable technique for surface wind reduction and improves upon the SF method that is similar to operational procedures for surface wind reduction. This model is selected for further detailed evaluation in the following section.

10.1029/2025JH000584

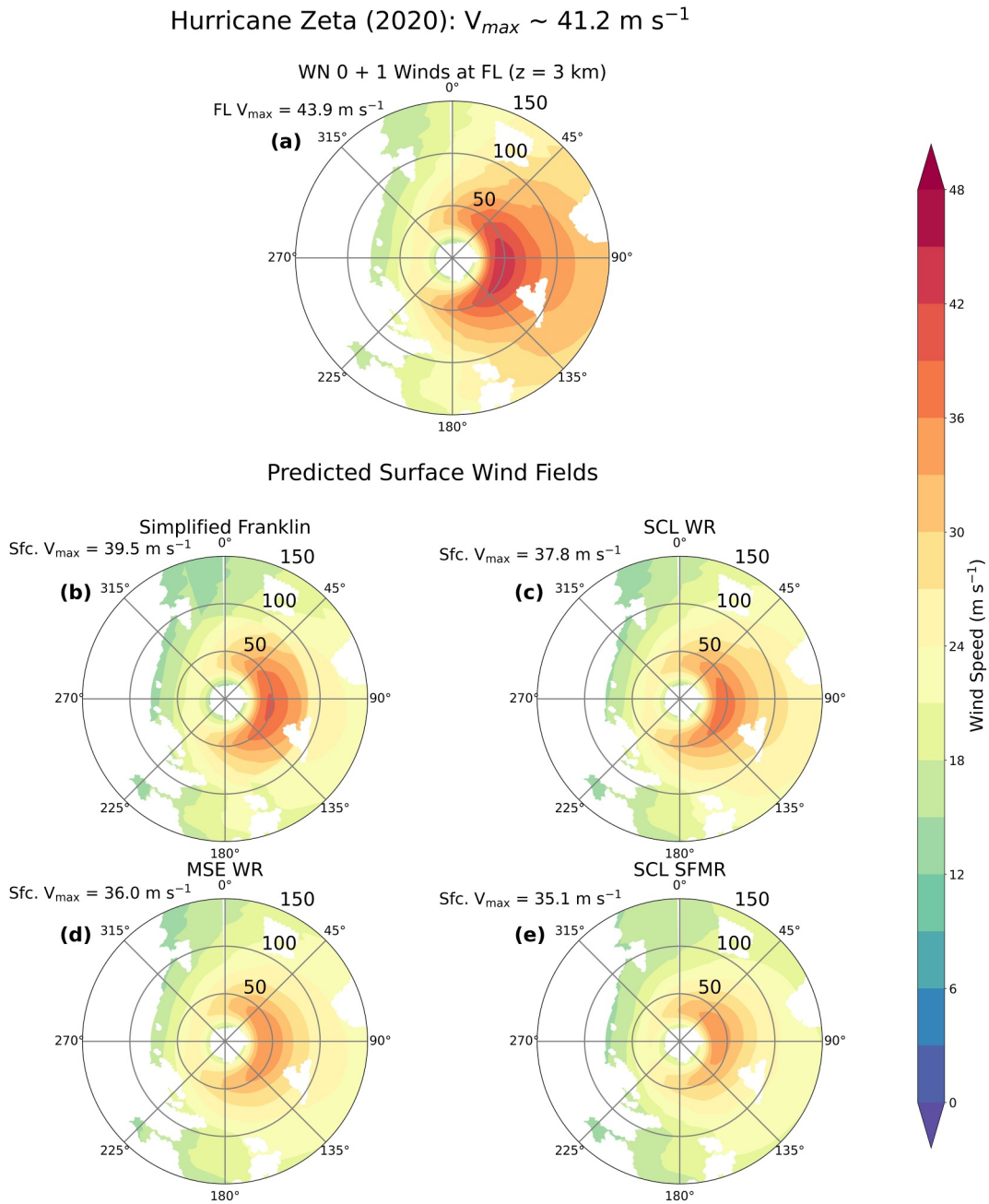

Figure 8. (a) Flight-level (FL) wind field at 3-km altitude from the Hurricane Zeta case in TC-RADAR collected near 12 UTC 28 August 2020 at Category 1 intensity with the maximum observed wind at FL given. Predicted surface wind fields are given for the (b) SF, (c) SCL WR, (d) MSE WR, (e) SCL SFMR techniques with the maximum surface wind speed in the predicted field.

3.3. Shifted Cubic Loss Wind Reduction Evaluation

Performance of the model on the FLIGHT+ data set is evaluated with the training, validation, and testing sets in Figure 10. The SCL WR model outperforms the SF technique in both linear correlation and RMSE in the training, validation, and testing sets. The change in performance between methods for each set is compared through changes in the scatter plots of predicted versus true SFMR values. Observations are grouped in 5 m s^{-1} bins between 10 and 85 m s^{-1} of true and predicted SFMR winds for each method. The bin counts for each method are subtracted (SCL WR - SF) and normalized across all sets based on the maximum increase and decrease of counts

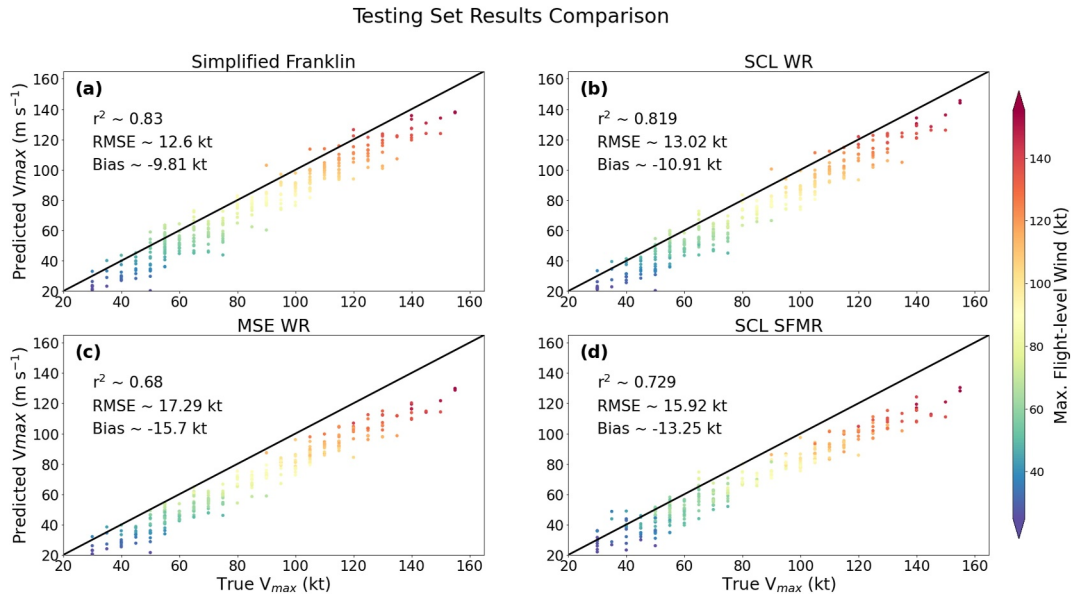

Figure 9. True V_{max} values versus predictions from the (a) SF, (b) SCL WR, (c) MSE WR, and (d) SCL SFMR. The maximum wind speed in each TC-RADAR analysis is shown (colorbar). The linear r^2 correlation value, root mean squared error (RMSE), and bias for each method is provided within each panel.

observed in each set (Figures 10c, 10f and 10i). The SCL WR model exhibits superior performance to the SF technique via the r^2 and RMSE metrics evaluated in the training, validation, and testing sets.

Since the SFMR values themselves have substantial uncertainties, the predicted surface wind values are compared against dropwindsonde observations from past reconnaissance flights for an independent verification. Since the

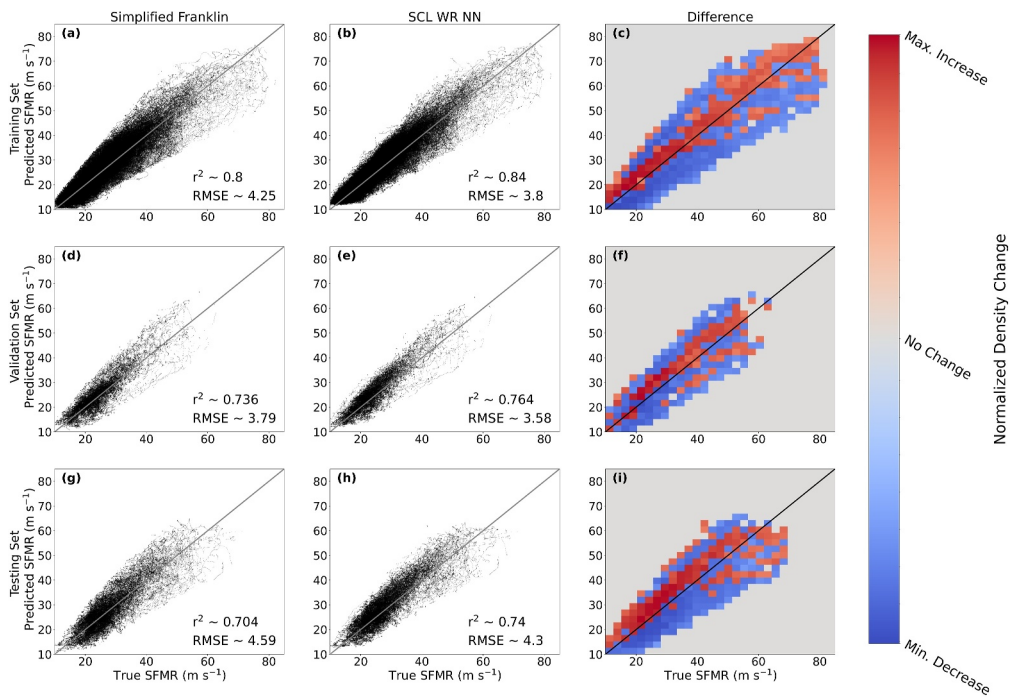

Figure 10. Predicted versus observed SFMR values with linear correlation (r^2) and root mean squared error (RMSE) values for the (a) SF and (b) SCL WR prediction techniques with a normalized density change (from SF to SCL WR) heat map (c) for the training, (d,e,f) validation, and (g,h,i) testing sets.

dropwindsondes are not collocated with the flight track, TC-RADAR analyses are used to produce 2-D maps of flight-level wind fields at 3-km altitude in storms of hurricane or greater strength and 1.5 km in storms of tropical storm strength, roughly corresponding to the 700 and 850 hPa pressure levels, respectively. The TC-RADAR analyses are merged across several radial flight legs to produce a single analysis for each flight. The collection of data over multi-hour periods increases spatial coverage of the wind-field analysis but results in temporal smoothing that reduces the maximum winds. Figure 11 shows the difference in surface wind values from the SF and SCL WR methods from collocated dropwindsonde WL150 values from TC-DROPS in the r^* and θ^* coordinate space for different TC intensities. For each intensity category, the errors are averaged in annular sectors defined by the θ^* bounds of the motion-relative quadrants (FL, FR, RR, and RL) and the r^* bounds of 0.3, 1.5, 3.0, and 5.0. Errors are expected for both methods due to temporal differences and differences between point measurements and the smoothed predictions from the merged radar inputs. However, it can be seen that the SCL WR method generally reduces the errors around the TC, especially to the left of the motion where the largest errors in the SF method tend to be observed. Corrections to left-of-motion under predictions are most notable in the inner core of systems of hurricane intensity or greater within 1.5 r^*.

Figure 12 shows the difference with dropwindsondes binned by observed surface wind speed in bins of 15–30, 30–45, 45–60, and >60 m s^{-1}. The 0–15 m s^{-1} bin is excluded since the model is not intended to reduce flight-level winds below 15 m s^{-1}; surface winds below 15 m s^{-1} are of lesser interest as the weakest forecast wind radii are 34 kt, or ∼ 17.5 m s^{-1} (Sampson & Knaff, 2015). Both methods show a dependence on wind speed, with a high bias at lower wind speeds and low bias at higher wind speeds. However, the SCL WR shows a reduction in RMSE compared to dropwindsonde WL150 in all wind speed bins. The differences are reduced the most at higher wind speeds, with a near-zero bias in the 45–60 m s^{-1} range for the SCL WR method. The SCL WR model still underestimates the surface winds of >60 m s^{-1}, but the sample size is small (42 points). The RMSE distribution was compared between the methods for each bin using the Mann-Whitney U two-tailed non-parametric test (Nachar, 2008). The only bin with a failure to reject the null hypothesis at the 95% confidence level is the 15–30 m s^{-1} bin where the difference in RMSE between the two methods is the smallest.

3.4. Evaluation of Real-Time Utility

These results show promise that the SCL WR method may be able to provide useful estimates of V_{max} with a surface wind field predicted from observed flight-level winds in real time. To improve the nomenclature, we dub the SCL WR method for real-time use as the Surface Winds from Aircraft with a Neural Network, or SWANN model. An example case from Hurricane Idalia (2023) is used to demonstrate the potential operational capability of the SWANN product. An aircraft collected TDR observations of Hurricane Idalia around 00 UTC 30 August 2023 at Category 2 intensity as it rapidly intensified in the Gulf of Mexico leading up to its landfall (Cangialosi & Alaka, 2024). Doppler radar data from the TDR, which are available in real time, are QCed with the method developed by Gamache et al. (2008). The TDR data are synthesized into a wind field using the Spline Analysis at Mesoscale Utilizing Radar and Aircraft Instrumentation (SAMURAI) software (Bell et al., 2012; Foerster & Bell, 2017), which has been optimized to run at speeds suitable for real-time analysis (Dennis et al., 2023).

The flight-level wind field at an altitude of 3 km is smoothed to WN 0 + 1 and then converted to the normalized polar coordinates of r^* and θ^* using the flight-level RMW. The predicted surface wind and WR fields are shown with the flight-level winds in Figure 13. The wind field is from one radial aircraft penetration through Idalia which takes on the order of an hour of flight time rather than the merged analysis which is over the course of several hours. The flight-level RMW is given as a dashed line, and the reduction factors have moved the surface wind maximum 2 km inward of the flight-level RMW, as is expected with an eyewall that slopes outward with height. The map of WR shows a left-to-right motion asymmetry consistent with boundary layer theory and asymmetric drag. The SWANN model yields a surface wind maxima which is ∼2 m s^{-1} below the operational estimate around this time, which is fairly accurate considering the smoothed radar-derived wind field.

4. Discussion and Conclusions

Tropical cyclone (TC) intensity and impacts depend on the surface wind field within the planetary boundary layer (PBL). These winds are rarely sampled directly by aircraft due to the dangers of flying in the turbulent PBL, but the maximum sustained wind (V_{max}) and other characteristics of the surface wind field must be diagnosed and forecast by operational forecast centers such as the NHC. The current NHC operational wind reduction (WR)

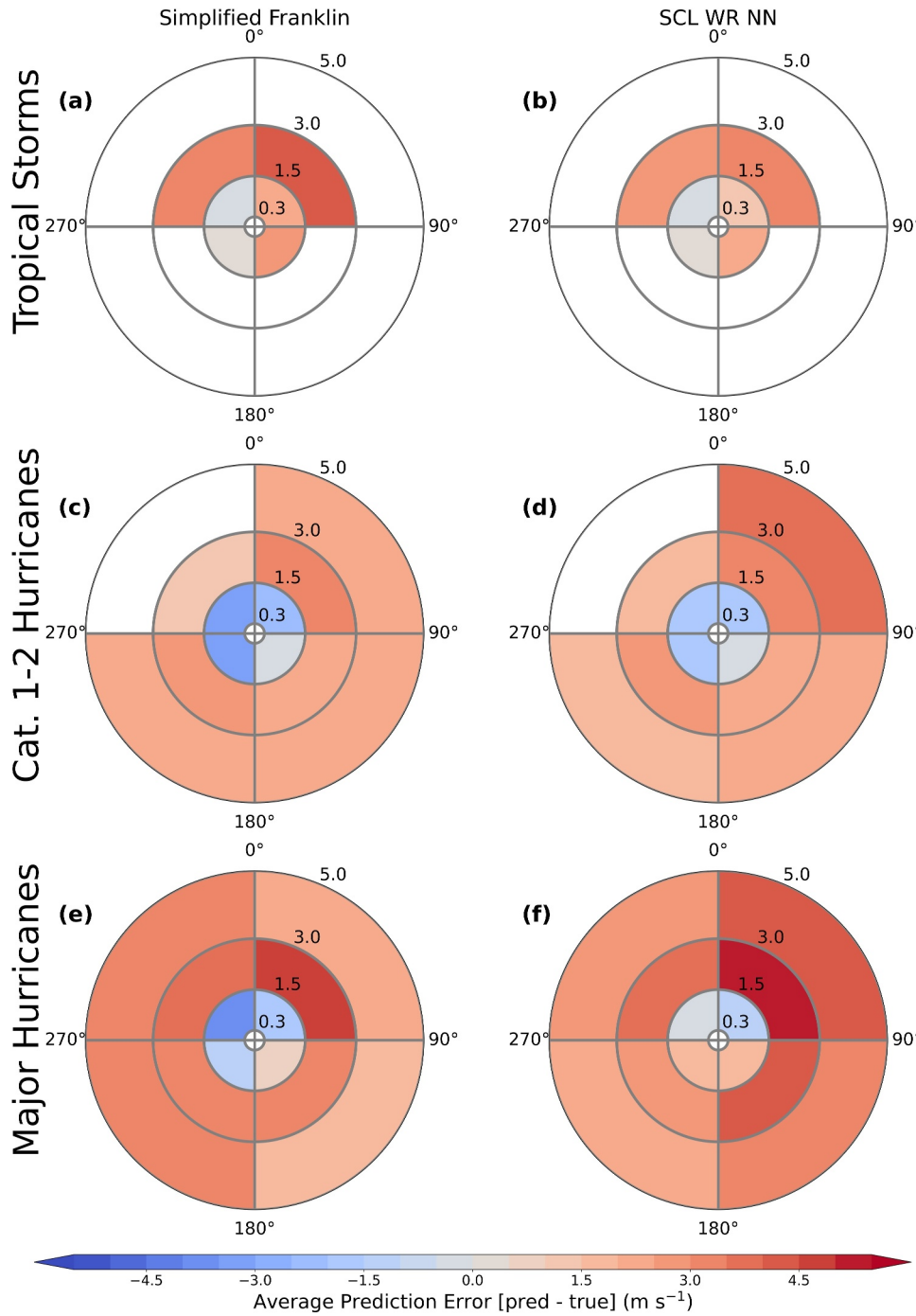

Figure 11. Errors (predicted - true; colorbar) of predicted surface winds with collocated surface wind dropsonde observations averaged in angular sectors of normalized polar coordinate space for the SF method in (a) tropical storms, (c) Category 1–2 hurricanes, and (e) major hurricanes. Errors are also given for the SCL WR NN method (b,d,f). Plotting bounds define the angular sectors for averaging. A lack of color within an angular sector indicates fewer than 10 dropsonde-prediction pairs could be found to produce an average.

procedure to estimate surface winds from aircraft flight-level data was derived from descending profile measurements of dropwindsondes in TCs by Franklin et al. (2003). A Simplified Franklin (SF) scheme is developed and used to interpolate operational WRs as a benchmark for comparison against results with neural network (NN) machine learning models. The SF WRs are limited by fixed values intended for point-wise application, which are

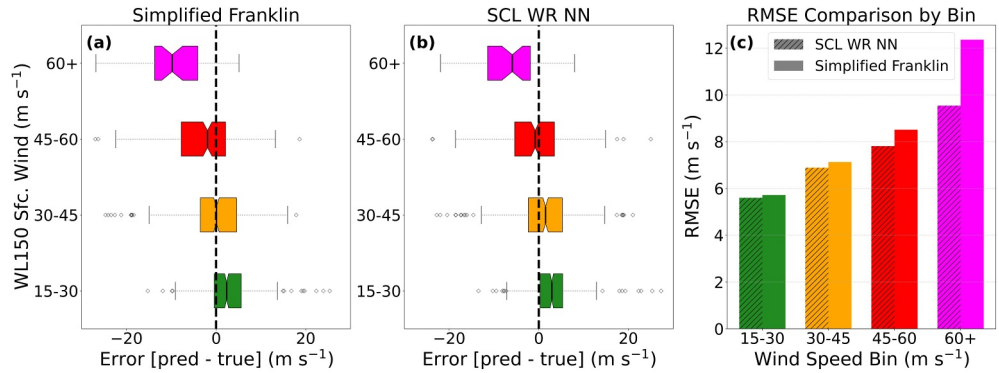

Figure 12. Box and whisker plots of errors (predicted - true) in surface wind predictions compared to dropsonde observations of surface winds in bins of 15–30 m s^{-1} (green; $n = 456$), 30–45 m s^{-1} (orange; $n = 413$), 45–60 m s^{-1} (red; $n = 240$), and >60 m s^{-1} (magenta; $n = 42$) for the (a) SF and (b) SCL WR techniques. The boxes represent the interquartile range (25th–75th percentiles) with the lines indicating the medians; the whiskers extend to the most extreme values within 1.5 times the interquartile range, and points represent outliers. (c) Root mean squared error values are compared for both methods given as bars that correspond to each bin.

incapable of characterizing complex asymmetric TC wind fields. In the current study we use the SFMR which can deduce surface wind speeds through a geophysical model function (GMF). The GMF needs continued improvement (Sapp et al., 2019), but the large volume of SFMR data enables new analysis and training of a NN model which can discern useful relationships for surface wind reduction amidst the large variability of the instrument observations.

Our results show that the SF method is broadly consistent with the mean observed WRs derived from SFMR data collected from the 2016 to 2019 hurricane seasons, but does not adequately capture the asymmetric WRs due in part to motion and frictional drag in the PBL (Kepert, 2001; Shapiro, 1983). Analyzing the distribution of WRs with respect to radius in storm-motion-relative quadrants in different intensity groups indicates WRs around the TC should change based on storm motion, intensity, and structure. Our analysis is consistent with Powell et al. (2009), who recommended wind reduction methodologies depending on inertial stability. Stronger and intensifying TCs also tend to have more peaked radial wind profiles at flight level (Martinez et al., 2017), which impact the wind structure in the PBL by driving stronger inflow (Williams, 2015). Inclusion of the most recent prior intensity estimate for a storm and the radial location of the flight-level RMW gives the NN additional information relevant to reducing the inner-core winds to the surface.

To account for variations in size and storm motion, the observed data are mapped to a polar grid defined by a radius (r^*) normalized by the radius of maximum wind (RMW) at flight level and storm-motion-relative azimuths (θ^*). The r^*, θ^*, and storm motion magnitude predictors give the NNs trained in this study necessary context to account for motion-relative asymmetries as well as other sources of variability expected in the TC inner core near the RMW. Several different NNs were trained and compared to predict surface wind or WRs with standard and

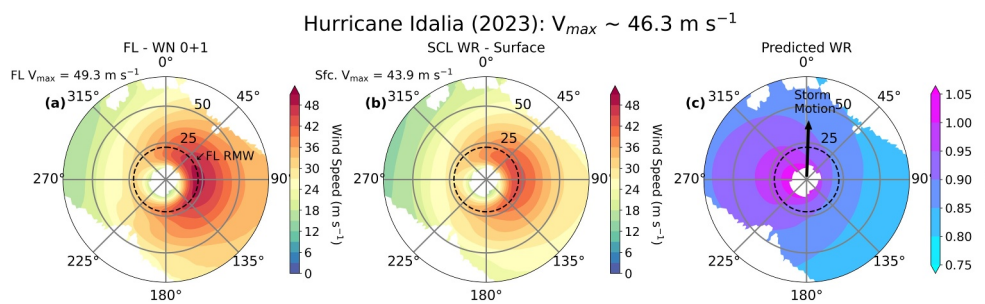

Figure 13. A pseudo-real-time product example of the SWANN model reducing the observed flight-level wind field in Hurricane Idalia near 00 UTC 30 August 2023 at Category 2 intensity. The (a) flight-level wind field at 3-km altitude, (b) predicted surface wind field and its maximum value, and (c) predicted WRs are shown with the flight-level radius of maximum wind (RMW) given as a dashed circle and storm motion direction (2°) as an arrow.

custom loss functions. The best performer of the different NN methodologies predicted WR and used a custom shifted cubic loss (SCL) function. The SCL function increases the loss penalty assessed on prediction errors for rare, but important, high-wind observations in the data set. The SCL WR method, dubbed the Surface Winds from Aircraft with a Neural Network (SWANN) model, produced the best balance of high accuracy of the surface wind compared to SFMR, low variance in predicted WRs, and low bias in high winds. The SWANN method exhibits a slight high bias at weaker winds below major hurricane force, but this counteracts, to some extent, a low bias of the SFMR GMF below 45 m s^{-1} and the systematic undersampling of V_{max} by the SFMR due to the inability to directly sample V_{max} with aircraft during every flight, especially in weaker TCs (Klotz & Nolan, 2019).

Although reducing absolute error compared to observations is generally beneficial, the known shortcomings of the SFMR training data underscore the dangers of learning the noise and biases of an imperfect observational data set. In addition to instrument noise, additional variance in WRs is expected due to turbulence in the PBL (Lorsolo et al., 2010). Smaller-scale features such as mesovortices can further complicate the problem by locally enhancing wind speeds near the eyewall of intense TCs (Cha et al., 2020). Despite the noise of the SFMR and physical variability in WRs, the SWANN model is still able to create a spatial map of WR that is consistent with PBL theory (Kepert, 2001) and produces physically reasonable and sufficiently smooth wind fields for forecasters. The adherence to the left-to-right asymmetry in basic theory as well as understanding of the eyewall slope provides evidence that SWANN is capable of finding relevant physical relationships present in the noisy observational data set. Improvements to the SFMR GMF are likely to continue which can improve the training data for this reduction method in the future, but additional understanding of sea surface behavior at high wind speeds will also be necessary (Holthuijsen et al., 2012). The NN trained by Eusbi et al. (2024), which was also tasked with capturing structural aspects of the TC wind field, was vastly improved by weighting their loss function using the wind speed magnitude. Their NN also benefited from physical knowledge by incorporating the Navier-Stokes equations into their loss function, which is an inventive and novel strategy. Additional constraints derived with the use of physical equations may be beneficial in a future version of the method.

To test the model on an independent data set beyond the training, validation, and testing sets, radar-derived flight-level wind fields from past reconnaissance flights are reduced to the surface by the SWANN and SF methods. The predicted surface winds are compared to collocated in-situ dropwindsonde measurements of near-surface winds from the same flights. Differences between dropwindsondes and the model-predicted winds shows improvement by SWANN over the SF method due to the ability of the model to accurately predict higher WRs left of storm motion. Differences are also reduced within the flight-level RMW, where WRs must be higher to predict the surface wind maximum located below weaker winds aloft due to the outward slope of the eyewall with height. The SWANN model has a lower root mean squared error (RMSE) than the SF method compared to dropwindsondes at all wind speeds from 15 m s^{-1} to >60 m s^{-1}. The model has a slight high bias at low wind speeds and a low bias at high wind speeds, but the greatest improvements in RMSE are achieved at the highest winds, which are important to intensity estimation in strong TCs.

A test case with Hurricane Idalia (2023) while it was rapidly intensifying leading up to its landfall demonstrates the potential of SWANN for real-time utility. The predicted surface wind field is weaker, but more symmetric than the one observed at flight level with a maxima located inward of the flight-level RMW, consistent with expectations based on PBL theory and prior observations. The maximum value of the predicted surface wind field is $\sim$ 2 m s^{-1} below the operational intensity estimate at the time of the flight and offers the advantage of predicting a full surface wind field compared to the method of Powell et al. (2009), which is meant to estimate the singular value of a maximum surface wind. Recent concerns with the quality of the operational stream of SFMR data, which led to a cessation of its transmission from NOAA P-3 aircraft in 2024 (National Hurricane Center, 2024), may ultimately necessitate a retraining of this method with revised data if issues are found to extend into past years. Interestingly, the ability of the SWANN model to learn physical relationships for WR from a noisy, but large SFMR data set could offer a useful substitute for real-time SFMR in future outages. The success of the model compared to independent dropwindsonde measurements and the SF method suggests that SWANN may not be negatively impacted by any systematic biases in the SFMR data set. Some wind-speed-dependent bias is still apparent in both the SF and SWANN methods indicating opportunities for improvement.

SWANN reasonably approximates some basic motion-induced asymmetric and eyewall-slope-related structure expected in WRs, but the method does not capture other more complex factors which impact WRs. Factors including, but not limited to, vertical wind shear (VWS), PBL turbulence, baroclinic influence, and mesovortices

may account for some of the perceived instrument noise in the observational data. Additional physically relevant predictors like VWS magnitude or information on convective activity could improve the accuracy of the method. However, additional predictors create dependencies on other data sources, so a balance must be maintained between added complexity and operational feasibility. Continued care must be taken with the addition of new predictors and evaluation of observational and instrument uncertainties of the training data. Additional cases, testing, and model development are recommended for SWANN to better characterize and reduce errors and biases for real-time intensity guidance and forecaster support.

Data Availability Statement

Information to access the TC-RADAR data set is available in Fischer et al. (2022). The FLIGHT+ data set is available online for users to register and download (Vigh et al., 2021). The TC-DROPS data set (Zawislak et al., 2018) is still in development prior to an upcoming official release, but the dropsonde data is publicly available from the NOAA Hurricane Research Division (HRD) archive (NOAA Hurricane Research Division, 2024). A repository containing relevant code to generate and run the model can be found on Figshare (DesRosiers et al., 2025).

Acknowledgments

This work is funded as part of the NOAA Hurricane and Ocean Testbed (HOT) program by award NA22OAR4590521 through the Colorado State University Cooperative Institute for Research in the Atmosphere (CIRA). A. DesRosiers and M. Bell were also supported by Office of Naval Research award N00014-20-1-2069. We would like to thank our collaborators on this project Jun Zhang, Wallace Hogsett, Lisa Bucci, Jason Sippel, and forecasters at NHC for their helpful comments on the research. We thank Wallace Hogsett for providing greater detail on the NHC operational wind reduction methodology used to create the Simplified Franklin method. We would also like to thank the U.S. Air Force and NOAA Hurricane Hunters for their tireless dedication to TC reconnaissance and the collection of data used in this study. FLIGHT+ was created by the Research Applications Laboratory at the National Science Foundation (NSF) National Center for Atmospheric Research (NCAR) from data provided by HRD and the U.S. Air Force Reserve. We thank Neal Dorst and Heather Holbach for their contributions to FLIGHT+. The initial creation of this data set was funded through a grant from the Bermuda Institute of Ocean Sciences Risk Prediction Initiative (RPI2.0). The extension of this data set was made possible due to substantial funding support from the NOAA Hurricane Forecast Improvement Project (HFIP) through Grant NA18NWS4680058, entitled "New Frameworks for Predicting Extreme Rapid Intensification." This material is based in part upon work supported by NSF NCAR, which is a major facility sponsored by the U.S. NSF under Cooperative Agreement No. 1852977.

References

Abadi, M., Barham, P., Chen, J., Chen, Z., Davis, A., Dean, J., et al. (2016). TensorFlow: A system for large-scale machine learning. *arXiv preprint arXiv:1605.08695*.

Bell, M. M., Montgomery, M. T., & Emanuel, K. A. (2012). Air–sea enthalpy and momentum exchange at major hurricane wind speeds observed during CBLAST. *Journal of the Atmospheric Sciences*, *69*(11), 3197–3222. https://doi.org/10.1175/JAS-D-11-0276.1

Beven, J. L., Berg, R., & Hagen, A. (2019). National Hurricane Center tropical cyclone report: Hurricane Michael (AL142018). *NHC Tech. Rep*. www.nhc.noaa.gov/data/tcr/AL142018_Michael.pdf

Blake, E., Berg, R., & Hagen, A. (2021). National Hurricane Center tropical cyclone report: Hurricane Zeta (AL282020). *NHC Tech. Rep*. www.nhc.noaa.gov/data/tcr/AL282020_Zeta.pdf

Boukabara, S.-A., Krasnopolsky, V., Steward, J. Q., Maddy, E. S., Shahroudi, N., & Hoffman, R. N. (2019). Leveraging modern artificial intelligence for remote sensing and NWP: Benefits and challenges. *Bulletin of the American Meteorological Society*, *100*(12), ES473–ES491. https://doi.org/10.1175/BAMS-D-18-0324.1

Cangialosi, J. P., & Alaka, L. (2024). National Hurricane Center tropical cyclone report: Hurricane Idalia (AL102023). *NHC Tech. Rep*. www.nhc.noaa.gov/data/tcr/AL102023_Idalia.pdf

Cha, T.-Y., Bell, M. M., Lee, W.-C., & DesRosiers, A. J. (2020). Polygonal eyewall asymmetries during the rapid intensification of Hurricane Michael (2018). *Geophysical Research Letters*, *47*(15), e2020GL087919. https://doi.org/10.1029/2020GL087919

Chang, P., & Jelenak, Z. (2024). Are the multitude of aircraft and satellite wind and wave measurements causing confusion or clarity? Some insights from NOAA/NESDIS satellite and aircraft products. Retrieved from www.weather.gov/media/tropical/IHC-2024-Presentations/Jelenak-NESDISSTAR.pdf. (Tropical Cyclone Operations and Research Forum (TCORF), 6 March 2024, Lakeland, FL).

Dennis, J. M., Baker, A. H., Dobbins, B., Bell, M. M., Sun, J., Kim, Y., & Cha, T.-Y. (2023). Enabling efficient execution of a variational data assimilation application. *The International Journal of High Performance Computing Applications*, *37*, 101–114. https://doi.org/10.1177/10943420221119

DesRosiers, A. J., & Bell, M. M. (2024). Airborne radar quality control with machine learning. *Artificial Intelligence for the Earth Systems*, *3*(1), e230064. https://doi.org/10.1175/AIES-D-23-0064.1

DesRosiers, A. J., Bell, M. M., & Cha, T.-Y. (2022). Vertical vortex development in Hurricane Michael (2018) during rapid intensification. *Monthly Weather Review*, *150*(1), 99–114. https://doi.org/10.1175/MWR-D-21-0098.1

DesRosiers, A. J., Bell, M. M., DeHart, J. C., Vigh, J. L., Rozoff, C. M., & Hendricks, E. A. (2025). Tropical cyclone surface wind reduction with a neural network. [dataset]. https://doi.org/10.6084/m9.figshare.28148177

Ebert-Uphoff, I., Lagerquist, R., Hillburn, K., Lee, Y., Haynes, K., Stock, J., et al. (2021). CIRA guide to custom loss functions for neural networks in environmental sciences – Version 1. *arXiv preprint arXiv:2106.09757*.

Eusbi, R., Vecchi, G. A., Lai, C.-Y., & Tong, M. (2024). Realistic tropical cyclone wind and pressure fields can be reconstructed from sparse data using deep learning. *Nature Communications Earth and Environment*, *5*(1), 8. https://doi.org/10.1038/s43247-023-01144-2

Fischer, M. S., Reasor, P. D., Rogers, R. F., & Gamache, J. F. (2022). An analysis of tropical cyclone vortex and convective characteristics in relation to storm intensity using a novel airborne Doppler radar database. *Monthly Weather Review*, *150*(9), 2255–2278. https://doi.org/10.1175/MWR-D-21-0223.1

Foerster, A. M., & Bell, M. M. (2017). Thermodynamic retrieval in rapidly rotating vortices from multiple-Doppler radar data. *Journal of Atmospheric and Oceanic Technology*, *34*(11), 2353–2374. https://doi.org/10.1175/JTECH-D-17-0073.1

Franklin, J. L., Black, M. L., & Valde, K. (2003). GPS dropwindsonde wind profiles in hurricanes and their operational implications. *Weather and Forecasting*, *18*(1), 32–44. https://doi.org/10.1175/1520-0434(2003)018⟨0032:GDWPIH⟩2.0.CO;2

Gamache, J. F., Dodge, P., & Griffin, N. (2008). Automatic quality control and analysis of airborne Doppler data: Realtime applications, and automatically post-processed analyses for research. In *Preprints, 28th conf. On hurricanes and tropical meteorology, Orlando, FL, Amer. Meteor. Soc., P2B (vol. 12)*.

Hazelton, A. T., & Hart, R. E. (2013). Hurricane eyewall slope as determined from airborne radar reflectivity data: Composites and case studies. *Weather and Forecasting*, *28*(2), 368–386. https://doi.org/10.1175/WAF-D-12-00037.1

Holbach, H. M. (2022). SFMR retrieval algorithm update. Retrieved from www.weather.gov/media/nws/IHC2022/SFMR_Updates_IHC.pdf. (Tropical Cyclone Operations and Research Forum (TCORF), 9 March 2022, Lakeland, FL).

Holthuijsen, L. H., Powell, M. D., & Pietrzak, J. D. (2012). Wind and waves in extreme hurricanes. *Journal of Geophysical Research*, *117*(C9). https://doi.org/10.1029/2012JC007983

Kepert, J. (2001). The dynamics of boundary layer jets within the tropical cyclone core. Part I: Linear theory. *Journal of the Atmospheric Sciences*, *58*(17), 2469–2484. https://doi.org/10.1175/1520-0469(2001)058⟨2469:TDOBLJ⟩2.0.CO;2

Kepert, J. (2023). A parametric model of tropical cyclone surface winds for sea and land. *Weather and Forecasting*, *38*(9), 1739–1757. https://doi.org/10.1175/WAF-D-23-0028.1

Kepert, J., & Wang, Y. (2001). The dynamics of boundary layer jets within the tropical cyclone core. Part II: Nonlinear enhancement. *Journal of the Atmospheric Sciences*, *58*(17), 2485–2501. https://doi.org/10.1175/1520-0469(2001)058⟨2485:TDOBLJ⟩2.0.CO;2

Klotz, B. W., & Nolan, D. S. (2019). SFMR surface wind undersampling over the tropical cyclone life cycle. *Monthly Weather Review*, *147*(1), 247–268. https://doi.org/10.1175/MWR-D-18-0296.1

Klotz, B. W., & Uhlhorn, E. W. (2014). Improved Stepped Frequency Microwave Radiometer tropical cyclone surface winds in heavy precipitation. *Journal of Atmospheric and Oceanic Technology*, *31*(11), 2392–2408. https://doi.org/10.1175/JTECH-D-14-00028.1

Knaff, J. A., Sampson, C. R., Kucas, M. E., Brennan, M. J., Meissner, T., Caroff, P., et al. (2021). Estimating tropical cyclone surface winds: Current status, emerging technologies, historical evolution, and a look to the future. *Tropical Cyclone Research and Review*, *10*(3), 125–150. https://doi.org/10.1016/j.tcrr.2021.09.002

Knaff, J. A., & Slocum, C. J. (2024). An automated method to analyze tropical cyclone surface winds from real-time aircraft reconnaissance observations. *Weather and Forecasting*, *39*(2), 339–349. https://doi.org/10.1175/WAF-D-23-0077.1

Landsea, C. W., & Franklin, J. L. (2013). Atlantic hurricane database uncertainty and presentation of a new database format. *Monthly Weather Review*, *141*(10), 3576–3592. https://doi.org/10.1175/MWR-D-12-00254.1

LeCun, Y., Bengio, Y., & Hinton, G. (2015). Deep learning. *Nature*, *521*, 436–444. https://doi.org/10.1038/nature14539

Lorsolo, S., & Aksoy, A. (2012). Wavenumber analysis of azimuthally distributed data: Assessing maximum allowable gap size. *Monthly Weather Review*, *140*(6), 1945–1956. https://doi.org/10.1175/MWR-D-11-00219.1

Lorsolo, S., Gamache, J., & Aksoy, A. (2013). Evaluation of the Hurricane Research Division Doppler radar analysis software using synthetic data. *Journal of Atmospheric and Oceanic Technology*, *30*(6), 1055–1071. https://doi.org/10.1175/JTECH-D-12-00161.1

Lorsolo, S., Zhang, J. A., Marks, F., & Gamache, J. (2010). Estimation and mapping of hurricane turbulent energy using airborne Doppler measurements. *Monthly Weather Review*, *138*(9), 3656–3670. https://doi.org/10.1175/2010MWR3183.1

Martinez, J., Bell, M. M., Vigh, J. L., & Rogers, R. F. (2017). Examining tropical cyclone structure and intensification with the FLIGHT+ dataset from 1999 to 2012. *Monthly Weather Review*, *145*(11), 4401–4421. https://doi.org/10.1175/MWR-D-17-0011.1

Nachar, N. (2008). The Mann-Whitney U: A test for assessing whether two independent samples come from the same distribution. *Tutorials in Quantitative Methods for Psychology*, *4*(1), 13–20. https://doi.org/10.20982/tqmp.04.1.p013

National Hurricane Center. (2024). Automated tropical cyclone forecast ATCF system public messages. Retrieved from https://ftp.nhc.noaa.gov/atcf/pns/pnsnhc.msg

NOAA Hurricane Research Division. (2024). HRD dropsonde archive. Retrieved from www.aoml.noaa.gov/ftp/pub/hrd/data/dropsonde/

O'Malley, T., Bursztein, E., Long, J., Chollet, F., Jin, H., & Invernizzi, L. (2019). Kerastuner. Retrieved from github.com/keras-team/keras-tuner

Powell, M. D., Uhlhorn, E. W., & Kepert, J. D. (2009). Estimating maximum surface winds from hurricane reconnaissance measurements. *Weather and Forecasting*, *24*(3), 868–883. https://doi.org/10.1175/2008WAF2007087.1

Sampson, C. R., & Knaff, J. A. (2015). A consensus forecast for tropical cyclone gale wind radii. *Weather and Forecasting*, *30*(5), 1397–1403. https://doi.org/10.1175/WAF-D-15-0009.1

Sapp, J. W., Alsweiss, S. O., Jelenak, Z., Chang, P. S., & Carswell, J. (2019). Stepped frequency microwave radiometer wind-speed retrieval improvements. *Remote Sensing*, *11*(3), 214. https://doi.org/10.3390/rs11030214

Shapiro, L. J. (1983). The asymmetric boundary layer flow under a translating hurricane. *Journal of the Atmospheric Sciences*, *40*(8), 1984–1998. https://doi.org/10.1175/1520-0469(1983)040⟨1984:TABLFU⟩2.0.CO;2

Srivastava, N., Hinton, G., Krizhevsky, A., Sutskever, I., & Salakhutdinov, R. (2014). Dropout: A simple way to prevent neural networks from overfitting. *Journal of Machine Learning Research*, *15*, 1929–1958.

Stern, D. P., Vigh, J. L., Nolan, D. S., & Zhang, F. (2015). Revisiting the relationship between eyewall contraction and intensification. *Journal of the Atmospheric Sciences*, *72*(4), 1283–1306. https://doi.org/10.1175/JAS-D-14-0261.1

Stewart, S. R. (2017). National Hurricane Center tropical cyclone report: Hurricane Matthew (AL142016). *NHC Tech. Rep*. www.nhc.noaa.gov/data/tcr/AL142016_Matthew.pdf

Uhlhorn, E. W., & Black, P. G. (2003). Verification of remotely sensed sea surface winds in hurricanes. *Journal of Atmospheric and Oceanic Technology*, *20*(1), 99–116. https://doi.org/10.1175/1520-0426(2003)020⟨0099:VORSSS⟩2.0.CO;2

Uhlhorn, E. W., Black, P. G., Franklin, J. L., Goodberlet, M., Carswell, J., & Goldstein, A. S. (2007). Hurricane surface wind measurements from an operational stepped frequency microwave radiometer. *Monthly Weather Review*, *135*(9), 3070–3085. https://doi.org/10.1175/MWR3454.1

Uhlhorn, E. W., Klotz, B. W., Vukicevic, T., Reasor, P. D., & Rogers, R. F. (2014). Observed hurricane wind speed asymmetries and relationships to motion and environmental shear. *Monthly Weather Review*, *142*(3), 1290–1311. https://doi.org/10.1175/MWR-D-13-00249.1

Vigh, J. L., Dorst, N. M., Williams, C. L., Stern, D. P., Uhlhorn, E. W., Klotz, B. W., et al. (2021). FLIGHT+: The extended flight level dataset for tropical cyclones (version 1.3). *Tropical Cyclone Data Project, National Center for Atmospheric Research, Research Applications Laboratory, Boulder, Colorado*. [dataset]. https://doi.org/10.5065/D6WS8R93

Williams, G. J. (2015). The effects of vortex structure and vortex translation on the tropical cyclone boundary layer wind field. *Journal of Advances in Modeling Earth Systems*, *7*(1), 188–214. https://doi.org/10.1002/2013MS000299

Zawislak, J., Nguyen, L., Paltz, E., Young, K., Voemel, H., & Hock, T. (2018). Development and applications of a long-term, global tropical cyclone dropsonde dataset. In *33rd conference on hurricanes and tropical metorology*. Amer. Meteor. Soc.

Zhang, J. A., Rogers, R. F., Nolan, D. S., & D, M. F. (2011). On the characteristic height scales of the hurricane boundary layer. *Monthly Weather Review*, *139*(8), 2523–2535. https://doi.org/10.1175/MWR-D-10-05017.1

Erratum

The originally published version of this article contained a typographical error. The unit m s^{-1} was mistakenly written as ms^{-1} in several instances throughout the article. The error has been corrected, and this may be considered the authoritative version of record.